Development/Plasticity/Repair

An Early Cortical Progenitor-Specific Mechanism Regulates Thalamocortical Innervation

Suranjana Pal,[1] Deepanjali Dwivedi,[2*] Tuli Pramanik,[1*] Geeta Godbole,[1] Takuji Iwasato,[3,4] Denis Jabaudon,[5] Upinder S. Bhalla,[2] and Shubha Tole[1]

[1]Department of Biological Sciences, Tata Institute of Fundamental Research, Mumbai, 400005, India, [2]National Centre for Biological Sciences, Tata Institute of Fundamental Research, Bengaluru, 560001, India, [3]Laboratory of Mammalian Neural Circuits, National Institute of Genetics, Mishima, 411-8540, Japan, [4]Department of Genetics, SOKENDAI (Graduate University for Advanced Studies), Mishima, 411-8540, Japan, and [5]Department of Basic Neurosciences, University of Geneva, 1211 Geneva, Switzerland; Department of Neurology, Geneva University Hospital, 1205 Geneva, Switzerland

The cortical subplate is critical in regulating the entry of thalamocortical sensory afferents into the cortex. These afferents reach the subplate at embryonic day (E)15.5 in the mouse, but "wait" for several days, entering the cortical plate postnatally. We report that when transcription factor LHX2 is lost in E11.5 cortical progenitors, which give rise to subplate neurons, thalamocortical afferents display premature, exuberant ingrowth into the E15.5 cortex. Embryonic mutant subplate neurons are correctly positioned below the cortical plate, but they display an altered transcriptome and immature electrophysiological properties during the waiting period. The sensory thalamus in these cortex-specific *Lhx2* mutants displays atrophy and by postnatal day (P) 7, sensory innervation to the cortex is nearly eliminated leading to a loss of the somatosensory barrels. Strikingly, these phenotypes do not manifest if LHX2 is lost in postmitotic subplate neurons, and the transcriptomic dysregulation in the subplate resulting from postmitotic loss of LHX2 is vastly distinct from that seen when LHX2 is lost in progenitors. These results demonstrate a mechanism operating in subplate progenitors that has profound consequences on the growth of thalamocortical axons into the cortex.

Key words: **Subplate; barrels; electrophysiology**

Significance Statement

Thalamocortical nerves carry sensory information from the periphery to the cortex. When they first grow into the embryonic cortex, they "wait" at the subplate, a structure critical for the guidance and eventual connectivity of thalamic axons with their cortical targets. How the properties of subplate neurons are regulated is unclear. We report that transcription factor LHX2 is required in the progenitor "mother" cells of the cortical primordium when they are producing their "daughter" subplate neurons, in order for the thalamocortical pathway to wait at the subplate. Without LHX2 function in subplate progenitors, thalamocortical axons grow past the subplate, entering the cortical plate prematurely. This is followed by their eventual attrition and, consequently, a profound loss of sensory innervation of the mature cortex.

Received Jan. 27, 2021; revised May 29, 2021; accepted June 8, 2021.

Author contributions: S.P., D.D., U.S.B., and S.T. designed research; S.P., D.D., T.P., and G.G. performed research; S.P., D.D., T.P., D.J., U.S.B., and S.T. analyzed data; S.P. and S.T. wrote the first draft of the paper; S.P., D.D., T.P., T.I., U.S.B., and S.T. edited the paper; S.P., D.J., and S.T. wrote the paper; T.I. contributed unpublished reagents/analytic tools.

This work was supported by Wellcome Trust-Department of Biotechnology India Alliance Early Career Fellowship IA/E/11/1/500402 to G.G.; MEXT Grant 16H06459 to T.I.; and Department of Biotechnology, Ministry of Science and Technology, India, PR8681 and Department of Atomic Energy, Government of India Project RTI4003 to S.T. We thank Edwin S. Monuki for the gift of *Lhx2*$^{lox/lox}$; Yuqing Li for the gift of Emx1Cre; Klaus-Armin Nave for the gift of NexCre; Elizabeth Grove for the gifts of *Cad6* and *Lhx9* plasmid DNA used for generating RNA probes; Gordon Fishell for pCAGG-IRES-eGFP plasmid DNA for *in utero* electroporation; Shital Suryavanshi and the animal house staff of the Tata Institute for Fundamental Research for excellent support; and Achira Roy, Anindita Sarkar, Ashwin Shetty, and Hari Padmanabhan for critical input on the manuscript.

*D.D. and T.P. contributed equally to this work.

The authors declare no competing financial interests.

Correspondence should be addressed to Shubha Tole at shubhatole@gmail.com.

https://doi.org/10.1523/JNEUROSCI.0226-21.2021

Copyright © 2021 the authors

Introduction

Sensory input reaches the neocortex via thalamocortical tract, and the precise topography and connectivity of this tract are critical to sensory processing. A key feature of cortical innervation by thalamocortical axons is a "waiting period" during which thalamic afferents enter the dorsal telencephalon while cortical neurogenesis is still underway, but "wait" within the cortical subplate for a period lasting several days in rodents, before innervating layer 4 of the cortex (Lund and Mustari, 1977; Rakić, 1977; Shatz and Luskin, 1986; Ghosh and Shatz, 1992; Herrmann et al., 1994; Auladell et al., 2000; Hevner, 2000). The importance of the subplate as an intermediate target of the thalamocortical afferents is well established from studies in which subplate neurons were either experimentally ablated or mispositioned/reduced because of genetic perturbations (for review, see Hoerder-

Suabedissen and Molnár, 2015). Thalamocortical afferents make synaptic contacts with the subplate (Herrmann et al., 1994), and electrical activity in the subplate is critical for correct thalamocortical innervation of the cortical plate at later stages (Ghosh et al., 1990; Catalano and Shatz, 1998; Kanold and Shatz, 2006; Tolner et al., 2012). Subplate neurons are born at embryonic day (E) 11.5 in the mouse from common progenitors that will later produce the neurons of the cortical plate (Molyneaux et al., 2007). However, the mechanisms that regulate the properties of the subplate neurons that are necessary for the waiting period are unclear because the regulatory processes in cortical progenitors that give rise to subplate neurons are poorly understood.

Previously, we reported a loss of the somatosensory barrels upon cortex-specific deletion of *Lhx2* (Shetty et al., 2013). Barrels are a prominent feature of the rodent somatosensory cortex, formed by local aggregates of layer 4 cortical neurons when thalamocortical afferents innervate the cortex (Woolsey and van der Loos, 1970). We found that the barrels are absent in postnatal brains when *Lhx2* is disrupted using an Emx1Cre line, which acts in cortical progenitors from E11.5 (Emx1Cre$^{11.5}$) (Shetty et al., 2013). In contrast, disruption of *Lhx2* using the postmitotic neuron-specific NexCre permits somatosensory barrels to be formed postnatally in layer 4, albeit with some deficits (Zembrzycki et al., 2015; Wang et al., 2017). Based on these two distinct phenotypes, we hypothesized that LHX2 function in cortical progenitors is required for the key aspects of thalamocortical axon development.

Here, we analyze thalamocortical axon projection defects when *Lhx2* is disrupted in cortical progenitors using Emx1Cre$^{11.5}$, focusing on the somatosensory projections. We find that, although there is extremely limited thalamocortical innervation detectable in the postnatal cortex of *Emx1Cre*$^{11.5}$*::Lhx2*$^{lox/lox}$ mice, there is a premature exuberant ingrowth of thalamocortical fibers into the cortical plate in the embryo at E15.5. These fibers extend through the cortical plate and reach the marginal zone. This is followed by atrophy of the prominent sensory ventrobasal nucleus (VB) of the thalamus, and eventual loss of thalamocortical innervation of the cortex. Using CreER-driven tamoxifen-inducible *Lhx2* deletion, we identify that loss of LHX2 from E11.5, but not from E12.5 or E13.5, recapitulates the premature ingrowth phenotype, implicating the subplate in this process, since it is born at E11.5. The subplate in *Emx1Cre*$^{11.5}$*::Lhx2*$^{lox/lox}$ brains expresses specific markers and occupies its appropriate position under the cortical plate but exhibits severe dysregulation of its transcriptome. In addition, the electrophysiological properties of these subplate neurons are perturbed compared with controls. Our results offer novel insights into mechanisms that operate in cortical progenitors that are necessary for proper subplate differentiation and for thalamocortical axon development and circuit assembly.

Materials and Methods

Mice. All animal protocols were approved by the Institutional Animal Ethics Committee of Tata Institute of Fundamental Research according to regulations devised by the Committee for the Purpose of Control and Supervision of Experiments on Animals. Noon of the day of vaginal plug was designated as embryonic day 0.5 (E0.5). Mouse embryos of either sex were harvested at E15.5, E17.5, E18.5, P0, P2, and P7. The following lines were obtained from JAX labs: tdTomato reporter Ai9 (strain name: B6. CgGt (ROSA)26Sortm9 (CAG-tdTomato) Hze/J; stock #007909), tamoxifen-inducible CreERT2 line (strain name: B6; 129- Gt (ROSA)26Sortm1 (Cre/ERT)Nat/J; stock #004847). The following lines were obtained from: Emx1Cre$^{11.5}$ [Yuqing Li, University of Florida (Jin et al., 2000)]; *Lhx2*$^{lox/lox}$ [Edwin Monuki, University of California (Mangale et al., 2008)]; NexCre [Klaus Nave, Max Planck Institute for Experimental Medicine (Goebbels et al., 2007)]; TCA-GFP or 5HTT-GFP/SERT-GFP, a BAC-transgenic line [Takuji Iwasato, National Institute of Genetics (Mizuno et al., 2014)].

The Emx1Cre$^{11.5}$ line (referred to as Emx1Cre^{YL} in Shetty et al., 2013) acts a day later than a commonly used Emx1Cre line that acts from E10.5 (Emx1Cre$^{10.5}$, referred to as Emx1Cre^{KJ} in Shetty et al., 2013). Using Emx1Cre$^{11.5}$ to disrupt *Lhx2* permits the neocortex to be specified (Shetty et al., 2013) instead of being transformed into an ectopic paleocortex, which is seen with Emx1Cre$^{10.5}$ (Chou et al., 2009). Although reduced in extent compared with controls, the *Emx1Cre*$^{11.5}$*::Lhx2*$^{lox/lox}$ cortex expresses molecular markers of all neocortical layers in the correct order (Shetty et al., 2013). Since Emx1Cre action is specific to the dorsal telencephalon, the Emx1Cre$^{11.5}$ permits the examination of disruption of *Lhx2* in neocortical progenitors from E11.5 without simultaneously affecting *Lhx2* expression in the thalamus, making it an ideal reagent to examine cortex-specific effects on thalamocortical innervation. *Lhx2* is expressed in progenitors and also in newly postmitotic cells (Telley et al., 2016). We confirmed that NexCre-mediated recombination of an Ai9 reporter labels the postmitotic subplate (see Fig. 5*D*), and *Lhx2* expression is barely detectable in the *NexCre::Lhx2*$^{lox/lox}$ brain (Zembrzycki et al., 2015; Wang et al., 2017).

Sample preparation. For histological procedures, embryonic brains were harvested in prechilled 1× PBS. Postnatal pups were anesthetized on ice before transcardial perfusion with 4% (wt/vol) PFA (Sigma Millipore) made in 0.1 M PB, pH 7.4. Brains were fixed in 4% PFA overnight at 4°C and equilibrated in 30% sucrose before sectioning.

Administration of tamoxifen. Tamoxifen (Sigma) dissolved in corn oil (20 mg/ml) was administered by oral gavage to pregnant *Lhx2*$^{lox/lox}$ dams at different time points as mentioned in the text, and embryos were harvested at E15.5. For each embryo, the extent of recombination was examined in one series of sections. Control embryos were littermates with one WT copy of the relevant gene. For *Lhx2*$^{lox/lox}$ mice, the tamoxifen dosage administered was 75 µg/g body weight.

In situ Hybridization (ISH). ISH was performed as follows: the sections were fixed in 4% PFA, washed in 1 × PBS, and treated with Proteinase K (1 µg/ml). Hybridization was performed overnight at 70°C in hybridization buffer (4× SSC, 50% formamide, and 10% SDS) containing different antisense RNA probes. Post-hybridization washes were performed at 70°C in Solution X (2× SSC, 50% formamide, and 1% SDS). These were followed by washes in 2× SSC, 0.2× SSC, and then TBS–1% Tween 20 (TBST). The sections were incubated in anti-digoxigenin Fab fragments (Roche) at 1:5000 in TBST overnight at 4°C. The color reaction was performed using NBT/BCIP (Roche) in NTMT (100 mM NaCl, 100 mM Tris-pH 9.5, 50 mM $MgCl_2$, and 1% Tween-20) according to the manufacturer's instructions.

Probe preparation. All probes were prepared by *in vitro* transcription using a kit from Roche as per the manufacturer's instructions. Templates for *Calb2, Chst2, CTGF, Hpca, Lhx2 exon2–3, Nrp2, Nurr1, Prox1*, and *SERT* were generated by PCR using specific primers from E15.5 (for *Lhx2 exon 2-3, Nurr1*), P0 (for *Hpca, Nrp2*), and P7 (for *Calb2, Chst2, CTGF, Prox1, SERT*) mouse brain cDNA (T7 polymerase promoter sequence was added to the reverse primer sequence). Template for *Cad6* and *Lhx9* was generated from plasmid DNA by restriction enzyme digestion. Calb2-forward, AGCACTTTGATGCTGACGGA, Calb2-reverse, AGGTGGTGAGCTGTTGGATG; Chst2-forward, CATCTTTGGGGCAGCCACTA, Chst2-reverse, CGAAAGGCTTG GAGGAGGAG; CTGF-forward, AGCGGTGAGTCCTTCCAAAG, CTGF-reverse, GTAATGGCAGGCACAGGTCT; Hpca-forward, CA GGACCTGCGAGAGAACAC, Hpca-reverse, CAGTCCTCTTTTCCG GGGTC; Lhx2 exon2-3-forward, CGCGGATCCACCATGCCGTCC ATCAGC, Lhx2 exon2-3-reverse, TAATACGACTCACTATAGGG; Nrp2-forward, AGAAGCCAGCAAGATCCACC, Nrp2-reverse, GGCC AGACTCCATTCCCAAA; Nurr1-forward, CAGTCCGAGGAGATG ATGCC, Nurr1-reverse, AACCATCCCAACAGCTAGGC; Prox1-forward, 5′-GCAGGCCTACTATGAGCCAG-3′, Prox1-reverse, 5′-TTG

ACCACCGTGTCCACAA-3′; SERT-forward, CAAAACGTCTGG CAAGGTGG, SERT-reverse, CATACGCCCCTCCTGATGTC.

Immunohistochemistry. Brains were sectioned (30 μm) using a freezing microtome, and sections were mounted on Superfrost Plus slides (Electron Microscopy Sciences). Sections were quenched with 0.1 M PB, pH 7.4, containing 50 mM NH_4Cl for 10 min followed by washing with 0.1 M PB containing 0.1% (v/v) Triton X-100 for 10 min. Sections were incubated in blocking solution containing 10% (v/v) horse serum (Invitrogen) in 0.1 M PB with 0.3% (v/v) Triton X-100 (Sigma) for 45 min at room temperature. The sections were then incubated overnight at 4°C in primary antibodies: biotinylated goat anti-GFP (1:400; Abcam, catalog #ab6658), mouse anti-RFP (1:200; Allele Biotech, catalog #ABP-MAB-RT008), rabbit anti-CPLX3 (1:200; Synaptic Systems, catalog #122302), and rabbit anti-cleaved Caspase-3 (1:200; Cell Signaling, catalog #9664S). The sections were then washed in 0.1 M PB, followed by incubation in secondary antibody for 1.5 h at room temperature. Secondary antibodies used were as follows: streptavidin Alexa-488 (1:800; Invitrogen, catalog #S32354) for GFP, goat anti-mouse antibody conjugated to Alexa-568 (1:400, Invitrogen, catalog #A11004) for RFP, and donkey anti-rabbit antibody conjugated to Alexa-647 (1:400, Invitrogen, catalog #A31573) for Complexin3 and cleaved Caspase-3. The slides were again washed with 0.1 M PB and mounted in Fluoroshield (Sigma). For cytochrome oxidase staining, free-floating sections (50 μm vibratome sections, Leica Microsystems, VT1000S) were placed in a solution of 0.6 mg/ml DAB, 0.3 mg/ml Cytochrome C (Sigma), 45 mg/ml sucrose in 0.1 M PBS at 37°C until staining appeared.

In utero electroporation. This procedure was used to visualize the thalamocortical tract at embryonic stages since the TCA-GFP line does not display GFP expression in the thalamocortical axons until postnatal day (P) 2. *In utero* electroporation was performed to transfect a GFP-expressing plasmid into the diencephalon of control and mutant embryos at E11.5, when the neurons of the VB nucleus are born.

All procedures conducted followed the guidelines prescribed by the Institutional Animal Ethics Committee. Timed pregnant *Lhx2*$^{lox/lox}$ dams with E11.5 embryos were anesthetized with isoflurane (4% induction, 3% during the surgery) followed by oral administration of Meloxicam (Melonex, United Pharmacies). Uterine horns were successively exposed after a midline laparotomy of 1 cm. Embryos were injected with 1-2 μl plasmid DNA solution dissolved in nuclease-free water with 0.1% Fast Green, into the third ventricle (for targeting the dorsal thalamus) through the uterine wall using a fine-glass microcapillary. pCAGG-IRES-eGFP (2 μg/μl, a gift from G. Fishell, Harvard Medical School) was injected, and plasmid DNA was prepared using Macherey Nagel Nucleobond Xtra MaxiPrep Kit (catalog #740414). Embryos were electroporated by holding their head between tweezers-style circular electrodes (3 mm diameter, BTX Harvard Apparatus, catalog #450487) across the uterus wall by delivering three pulses (34 V, 40 ms duration with 999 ms intervals) with a square-wave electroporator (Nepagene CUY21). The uterine horns were returned into the abdominal cavity, the incision was sutured, and the embryos were allowed to continue their normal development until E15.5. The uterine horns and the abdominal cavity were kept moist throughout the surgery (20-25 min) by flushing 0.9% NaCl (prewarmed to 37°C). Animals were kept on a 37°C warm plate for 30 min for postsurgical recovery. An oral suspension of Meloxicam (Melonex, United Pharmacies) was mixed with the water in the feeding bottles of the dams (0.6 μl/ml) as an analgesic and given to the animals until 2 d after surgery.

Imaging. Bright-field images were taken using a Carl Zeiss Axioplan 2 + microscope, Nikon Digital Sight DS-F12 camera, and Nikon NIS 4.0 imaging software. Images of immunohistochemistry slides were obtained using a Carl Zeiss LSM 710 and LSM 880 imaging system. Image stacks were processed using ImageJ (National Institutes Health) (Schindelin et al., 2012) and ZEN 2.1 (black) software. Confocal images of multiple fields were acquired using tile-scanning mode using a motorized stage and were stitched using Zen2.1 software. Low-magnification images were acquired using 10× objective, and high-magnification images were acquired at 40× objective. Exposure, *z*-stack (20 μm) and gain settings were uniform across all tile images taken for a given composite image. Figure panels were prepared using Adobe Photoshop CS6 and Adobe Illustrator.

Microdissection. P0 brains were dissected in ice-cold HBSS, and 200-μm-thick sections were cut using a vibratome (VT1000S). The lowermost part of the cortical plate (presumptive subplate) was visually identified and micro-dissected under stereomicroscopic guidance in ice-cold HBSS under RNase-free conditions. Micro-dissected subplate tissue was stored in Buffer RLT Plus (QIAGEN) at −80°C, and RNA was extracted using RNeasy PLUS Micro kit (QIAGEN).

RNA sequencing. RNA sequencing was performed by Medgenome Technologies. mRNA was isolated from total RNA, cDNA was prepared, and libraries were prepared using the IlluminaTruSeq RNA Sample preparation V2. Libraries were multiplexed and sequenced as 100 bp pair-end reads using the Illumina HiSEQ2500 platform, at an expected depth of 60 M single reads. Sequenced reads were aligned on the latest mouse reference genome assembly (mm10) using HISAT2, SAM/BAM files were further processed using SAMtools, and the number of reads per transcript was calculated and normalized by DESeq2 using R software (Love et al., 2014). Genes were considered significantly differentially expressed for FDR of <0.1. For representation, genes with fold change cutoff of ±1.5 were used. Mutually exclusive and overlapping genes between datasets were identified using Venny (2.1.0). Gene ontology analysis was performed using Gene Ontology Resource (http://geneontology.org/). The RNA-seq data generated in this study have been deposited in the GEO database under accession number GSE159006.

Electrophysiology. Brain slices were prepared as described previously (Hirsch and Luhmann, 2008). Briefly, E15.5 embryos and P0-P1 *Lhx2*$^{lox/lox}$ and *Emx1Cre*$^{11.5}$*::Lhx2*$^{lox/lox}$ mouse pups were anesthetized by hypothermia and decapitated. Coronal slices (400 μm thick), including the primary somatosensory cortex, were cut in ice-cold aCSF (Hirsch and Luhmann, 2008) on a vibratome (VT1200S). Slices were allowed to equilibrate in oxygenated aCSF for 30 min in a storage chamber before being transferred to the submerged type recording chamber at 30°C-34°C. During preparation and recording procedures, slices were maintained in aCSF containing the following (in mM): 124 NaCl, 26 $NaHCO_3$, 3 KCl, 1.6 $CaCl_2$, 1.8 $MgCl_2$, 1.25 NaH_2PO_4, and 20 D-glucose, pH 7.4, after equilibration with 95% O_2−5% CO_2 (osmolarity 333 mOsm). The subplate neurons were visualized using infrared differential interference contrast optics using a 40× objective (water immersion lens, 0.9 NA) on an Olympus BX1WI microscope. They were identified by their location, morphology, and electrophysiological properties (Hirsch and Luhmann, 2008). Subplate neurons had typical horizontal bipolar morphologies and were located between the cell-dense cortical plate with radially oriented neurons and the cell-sparse white matter. Whole-cell patch-clamp recordings in current-clamp mode were obtained with an Axopatch 200B amplifier (Molecular Devices) and patch-pipettes (3-5 MΩ resistance) filled with the following (in mM): K-gluconate 155, $MgCl_2$ 2, NaHEPES 10, Na-PiCreatine 10, Mg_2-ATP_2 and Na_3-GTP 0.3, pH 7.3 (300 mOsm), and 2 mg/ml Biocytin (Sigma) for *post hoc* anatomical staining. Series resistance and input resistance were continuously monitored during the experiment, and the cell was discarded if these parameters changed by >25%. Slices were perfused at all times with aCSF at a flow rate of 2-3 ml/min. Electrophysiological recordings were digitized using Digidata 1400A. Current-clamp recordings were filtered at 10 kHz and sampled at 20 kHz. All analysis was done using custom-written code in MATLAB (R2013a) and Clampfit (10.7.0.3), and plots were made in GraphPad Prism software. Input resistance was measured by computing slope of the *I-V* curve obtained by current injections from –10 pA to 10 pA, in steps of 5 pA.

Experimental design and statistical analysis. The thalamocortical pathway phenotype we report in *Emx1Cre*$^{11.5}$*::Lhx2*$^{lox/lox}$ mice is 100% penetrant. Together, 92 *Emx1Cre*$^{11.5}$*::Lhx2*$^{lox/lox}$ brains, 12 *CreERT2::Lhx2*$^{lox/lox}$ brains, 15 *NexCre::Lhx2*$^{lox/lox}$ brains, and 87 control brains were analyzed for this study. Animals of both sexes were examined. The *Emx1Cre*$^{11.5}$ allele was always maintained in a hemizygous condition. Therefore, each litter produced ~50% controls without the Cre transgene. These littermate controls were used wherever possible. We did not find any variation between litters at any given stage. The detailed breakup of embryos/pups for each experiment/quantification is below:

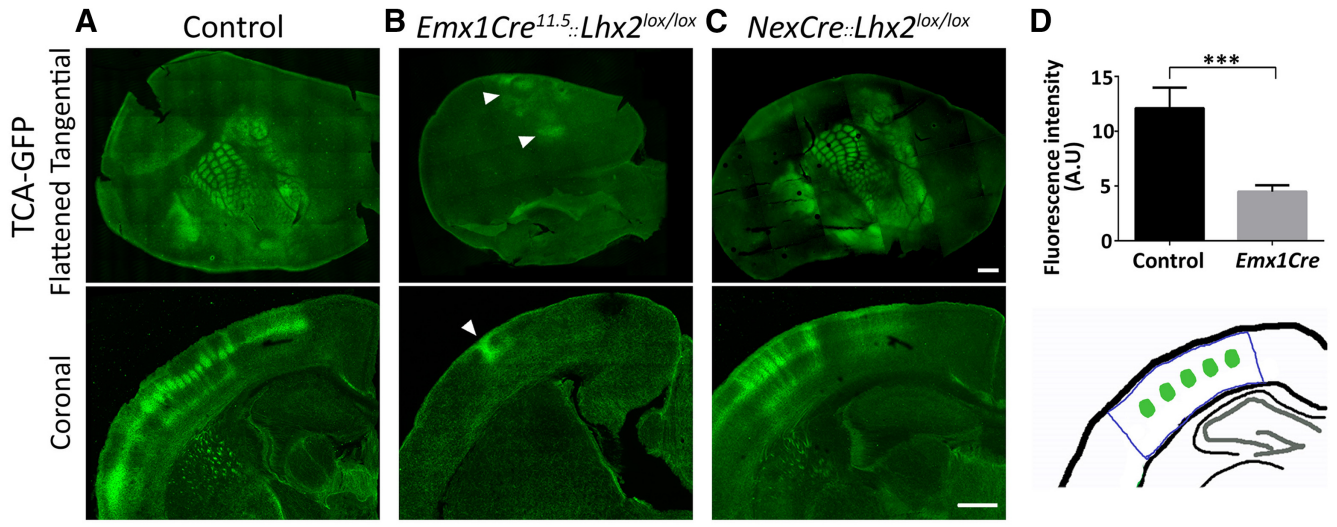

Figure 1. Emx1Cre-mediated loss of *Lhx2* causes severe disruption of the somatosensory barrels. ***A***, TCA-GFP reporter expression reveals the thalamocortical innervation and somatosensory barrels in flattened tangential sections and coronal sections at P7 in control brains. ***B***, In *Emx1Cre*$^{11.5}$*::Lhx2*$^{lox/lox}$*::TCA-GFP* brains, aberrant thalamocortical innervation (arrowheads) is seen clustered in a limited region of the cortex at P7. ***C***, *NexCre::Lhx2*$^{lox/lox}$*::TCA-GFP* brains reveal that postmitotic deletion of *Lhx2* permits thalamocortical afferents to innervate layer 4 and barrels can be detected. ***D***, Fluorescence intensity of the somatosensory cortex, measured in coronal sections, is significantly reduced in P7 *Emx1Cre*$^{11.5}$*::Lhx2*$^{lox/lox}$ brains compared with controls. Unpaired two-tailed Student's *t* test, ***$p = 0.0001$; $n = 5$ for each genotype. Tangential and coronal TCA-GFP images in ***A-C*** are composites of multiple confocal images. Scale bars, 500 μm.

Figure 1:

$n = 5$ for control and *Emx1Cre*$^{11.5}$*::Lhx2*$^{lox/lox}$.

$n = 3$ for *NexCre::Lhx2*$^{lox/lox}$. Our results were consistent with the phenotype for this genotype already published by other groups (Zembrzycki et al., 2015; Wang et al., 2017).

For quantification, three sections spanning the somatosensory cortex were scored in each brain. The fluorescent intensity of axonal terminals marked by TCA-GFP was measured in coronal sections using ImageJ in the area shown in the diagram (Fig. 1*D*). The fluorescence intensity was computed as the corrected pixel intensity difference between the "integrated density" of the selected area and the mean fluorescence of background readings from the same area, using functions available in ImageJ.

Figure 2:

Area measurements of the thalamus/thalamic nuclei: $n = 6$ for ages E17.5-E18.5; $n = 5$ for P0; $n = 3$ for ages P2-P7 for each genotype. For each embryo, VB/dLGN/dorsal thalamus area measurements were taken from three sections spanning the rostro-caudal extent of the structure using ImageJ software. The average mutant value was normalized to that of the average control value.

For thalamic nuclei markers/cytochrome oxidase/cCaspase3 staining, a total of 12 control and 12 mutant brains were examined for each genotype, and each marker was examined in at least three brains.

Figures 3 and 4:

For each condition, three embryos with the most extensive thalamic electroporation and no mis-targeting in the cortex were selected for quantification. Examples of the extent of thalamic electroporation are in Figure 3*A*. In each embryo, electroporated fibers were seen in the cortex in 2 or 3 contiguous sections. To maintain consistency, 2 sections with the most thalamocortical fibers labeled were scored. The area occupied by aberrant axonal branches (pink solid lines in the diagram) was measured using ImageJ, and normalized to the area of the cortical plate (dark gray region in the diagram) in mutants and controls.

Cortical thickness (Fig. 3*B*) was measured in the same sections scored for thalamocortical afferent ingrowth (Fig. 3*G*). The mutant value was normalized to that of the control value.

Figure 5:

For each genotype, 8 (P7) and 5 (E15.5) brains were analyzed for subplate markers. *Lhx2* expression was examined in serial sections.

Figure 6:

Micro-dissected tissue was pooled from 8 slices (four slices each from 2 brains) for each replicate sample. Two replicates each of control, *Emx1Cre*$^{11.5}$*::Lhx2*$^{lox/lox}$ and *NexCre::Lhx2*$^{lox/lox}$, were processed for RNA sequencing after ascertaining that their RIN values were >8.

Figures 7 and 8:

For E15.5, 14 cells from 7 control brains and 17 cells from 10 mutant brains were examined. For P0-P1, 16 cells from 5 control brains and 17 cells from 5 mutant brains were examined.

Statistical analysis. Statistical tests were performed using GraphPad Prism software version 8.3.0 (538) for Windows, GraphPad Prism Software. All the data were plotted as mean ± SEM. Results are indicated as significant if the *p* value is $p \leq 0.05$ (*), $p \leq 0.01$ (**), $p \leq 0.001$ (***), or $p \leq 0.0001$ (****).

Figure 1*D*: Statistical test: Unpaired two-tailed Student's *t* test, ***$p = 0.0001$; $n = 5$ for both control and *Emx1Cre*$^{11.5}$*::Lhx2*$^{lox/lox}$ brains.

Figure 2*G*: Ordinary one-way ANOVA with Fisher's LSD test, $F = 12.13$, ****$p < 0.0001$. E17.5 Control versus Mutant, *$p = 0.0153$; E18.5 Control versus Mutant, **$p = 0.0015$; P0 Control versus Mutant, ****$p < 0.0001$; P2 Control versus Mutant, ***$p = 0.0004$; P7 Control versus Mutant, ****$p < 0.0001$.

Figure 2*I*: Ordinary one-way ANOVA with Fisher's LSD test, $F = 4.171$, **$p < 0.01$. E18.5 Control versus Mutant, not significant, $p = 0.3130$; P0 Control versus Mutant, not significant, $p = 0.9271$; P2 Control versus Mutant, *$p = 0.0248$; P7 Control versus Mutant, **$p = 0.0017$.

Figure 2*J*: Ordinary one-way ANOVA with Fisher's LSD test, $F = 3.812$, **$p < 0.01$. E17.5 Control versus Mutant, not significant, $p = 0.2500$; E18.5 Control versus Mutant, not significant, $p = 0.0972$; P0 Control versus Mutant, not significant, $p = 0.5742$; P2 Control versus Mutant, not significant, $p = 0.3111$; P7 Control versus Mutant, ***$p = 0.0001$.

Figure 3*B*: Ordinary one-way ANOVA with Holm-Sidak's multiple comparisons test, $F = 0.6267$, not significant, $p = 0.6007$; Control versus *Emx1Cre*$^{11.5}$*::Lhx2*$^{lox/lox}$, not significant, $p > 0.9999$; Control versus *NexCre::Lhx2*$^{lox/lox}$, not significant, $p = 0.8440$; *Emx1Cre*$^{11.5}$*::Lhx2*$^{lox/lox}$ versus *NexCre::Lhx2*$^{lox/lox}$, not significant, $p = 0.8440$.

Figure 3*G*: Ordinary one-way ANOVA with Holm-Sidak's multiple comparisons test, $F = 67.14$, ****$p < 0.0001$; Control versus *Emx1Cre*$^{11.5}$*::Lhx2*$^{lox/lox}$, ****$p < 0.0001$; Control versus *NexCre::Lhx2*$^{lox/lox}$, not significant, $p = 0.9992$; *Emx1Cre*$^{11.5}$*::Lhx2*$^{lox/lox}$ versus *NexCre::Lhx2*$^{lox/lox}$, ****$p < 0.0001$.

Figure 4*G*: Ordinary one-way ANOVA with Holm-Sidak's multiple comparisons test, $F = 67.14$, ****$p < 0.0001$; Control versus *Emx1Cre*$^{11.5}$*::Lhx2*$^{lox/lox}$, ****$p < 0.0001$; Control versus *CreERT2::*

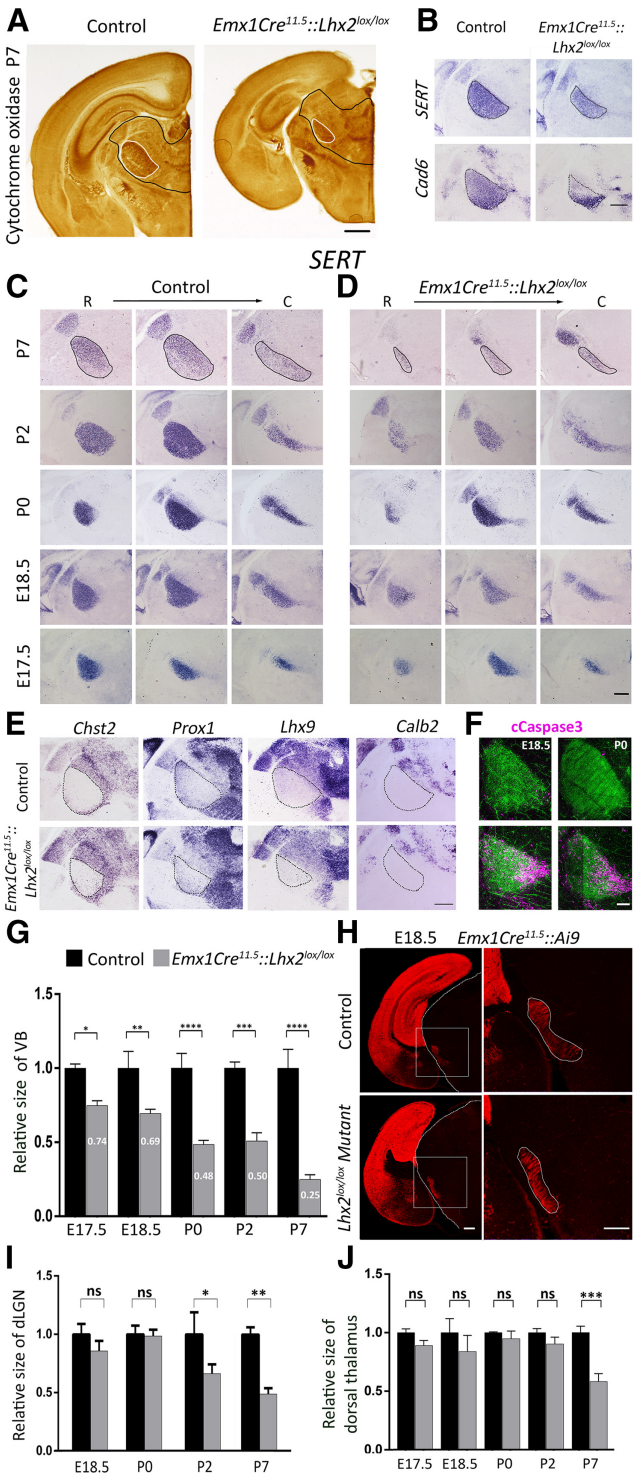

Figure 2. Emx1Cre-mediated loss of *Lhx2* causes shrinkage of the somatosensory VB nucleus from embryonic stages. ***A–H***, A comparison of control and *Emx1Cre*$^{11.5}$*::Lhx2*$^{lox/lox}$ mutant thalamus. ***A***, Cytochrome oxidase staining at P7 reveals a greatly shrunken VB (white ovals) and dorsal thalamus (black outline) on cortex-specific loss of *Lhx2*. ***B***, ***E***, The VB shrinkage is apparent at P0 by *SERT* and *Cad6* expression within this nucleus (black ovals, ***B***) and *Chst2*, *Prox1*, *Lhx9*, and *Calb2* expression along its borders and in other sensory nuclei (black ovals, ***E***). ***C***, ***D***, ***G***, Examination of *SERT* expression in control and mutant brains from E17.5-P7 brains reveals that the shrinkage of the VB is apparent from E17.5. Area measurements were quantified and compared in ***G*** using ordinary one-way ANOVA; E17.5, $*p = 0.0153$; E18.5, $**p = 0.0015$; P0, $****p < 0.0001$; P2, $***p = 0.0004$; P7, $****p < 0.0001$. $n = 6$ for ages E17.5-E18.5; $n = 5$ for P0; $n = 3$ for ages P2-P7 for each genotype. ***F***, Cleaved Caspase-3 immunostaining indicates increased cell death in the VB nucleus at E18.5 and P0 on cortex-specific loss of LHX2. ***H***, An Ai9 reporter (red) reveals that corticothalamic axons in both control and *Emx1Cre*$^{11.5}$*::Lhx2*$^{lox/lox}$ brains have reached the reticular thalamic nucleus at E18.5 (white solid lines), but have not yet innervated the VB nucleus. Scale bars: ***A-E***, ***H***, 500 µm; high-magnification images in ***F***, 200 µm. ***I***, ***J***, Quantification of dLGN area (***I***) and the total dorsal thalamus area (***J***). A comparison of the average values from control and *Emx1Cre*$^{11.5}$*::Lhx2*$^{lox/lox}$ brains reveals a shrinkage of these structures in *Emx1Cre*$^{11.5}$*::Lhx2*$^{lox/lox}$ brains at P2 and P7 (dLGN) and P7 (dorsal thalamus). $n = 3$ brains for each age and genotype. ***I***, Ordinary one-way ANOVA; E18.5, not significant, $p = 0.3130$; P0, not significant, $p = 0.9271$; P2, $*p = 0.0248$; P7, $**p = 0.0017$. ***J***, Ordinary one-way ANOVA; E17.5, not significant, $p = 0.2500$; E18.5, not significant, $p = 0.0972$; P0, not significant, $p = 0.5742$; P2, not significant, $p = 0.3111$; P7, $***p = 0.0001$.

Lhx2$^{lox/lox}$ Tam E11.5, $****p < 0.0001$; *Emx1Cre*$^{11.5}$*::Lhx2*$^{lox/lox}$ versus *CreERT2::Lhx2*$^{lox/lox}$ Tam E11.5, not significant, $p = 0.9969$; *CreERT2::Lhx2*$^{lox/lox}$ Tam E11.5 versus *CreERT2::Lhx2*$^{lox/lox}$ Tam E12.5, $****p < 0.0001$; *CreERT2::Lhx2*$^{lox/lox}$ Tam E11.5 versus *CreERT2::Lhx2*$^{lox/lox}$ Tam E12.75, $****p < 0.0001$; *CreERT2::Lhx2*$^{lox/lox}$ Tam E11.5 versus *CreERT2::Lhx2*$^{lox/lox}$ Tam E13.5, $****p < 0.0001$; *CreERT2::Lhx2*$^{lox/lox}$ Tam E12.5 versus *CreERT2::Lhx2*$^{lox/lox}$ Tam E12.75, not significant, $p = 0.4386$; *CreERT2::Lhx2*$^{lox/lox}$ Tam E12.5 versus *CreERT2::Lhx2*$^{lox/lox}$ Tam E13.5, not significant, $p = 0.3098$; *CreERT2::Lhx2*$^{lox/lox}$ Tam E12.75 versus *CreERT2::Lhx2*$^{lox/lox}$ Tam E13.5, not significant, $p = 0.9989$.

Results

In order to visualize thalamocortical projections, we used a TCA-GFP reporter line in which the expression of membrane-bound enhanced GFP is driven in primary sensory thalamic nuclei under serotonin transporter (*SERT*) promoter (Mizuno et al., 2014). The TCA-GFP background allowed us to compare the two *Lhx2* conditional mutants that were previously reported to have defects in thalamocortical innervation in postnatal brains: a complete loss of somatosensory barrels (*Emx1Cre*$^{11.5}$*::Lhx2*$^{lox/lox}$) (Shetty et al., 2013) or defects in polarized dendritic extension of layer 4 spiny stellate neurons (*NexCre::Lhx2*$^{lox/lox}$) (Wang et al., 2017).

Postnatal day (P) 7 brains were examined for GFP fluorescence indicative of thalamocortical innervation in either tangential slices of the cortex or coronal sections of hemispheres. The barrel map was visible in control brains (Fig. 1*A*), but was profoundly disrupted in *Emx1Cre*$^{11.5}$*::Lhx2*$^{lox/lox}$ brains, in which tangential slices revealed extremely reduced innervation in unstructured clusters that did not form any recognizable barrel field pattern (Fig. 1*B*, arrowheads). In contrast, barrels were still apparent in *NexCre::Lhx2*$^{lox/lox}$ brains (Fig. 1*C*). Coronal sections of *Emx1Cre*$^{11.5}$*::Lhx2*$^{lox/lox}$ brains showed the GFP-expressing axons to be clustered at one location and projecting aberrantly up to the marginal zone of the cortex, instead of layer 4. Quantification of the fluorescence intensity in the somatosensory cortex revealed a significant reduction in *Emx1Cre*$^{11.5}$*::Lhx2*$^{lox/lox}$ brains compared with controls (Fig. 1*D*).

The VB nucleus of the thalamus projects to the barrel cortex, and its neurons require the establishment of stable synapses with their layer 4 targets for survival (Zembrzycki et al., 2013; Greig et al., 2016). Therefore, we examined cytochrome oxidase staining in the P7 thalamus. The sensory thalamus as a whole and the VB nucleus in particular displayed a marked shrinkage in size in *Emx1Cre*$^{11.5}$*::Lhx2*$^{lox/lox}$ mutant brains (Fig. 2*A*). The VB nucleus, identified by the expression of *SERT* and *Cad6*, appeared shrunk at P0 as well (Fig. 2*B*) (Lebrand et al., 1996). To ascertain the time course of this shrinkage, we examined a range of ages and measured the VB area at three rostro-caudal levels. These area quantifications revealed that the VB is smaller in

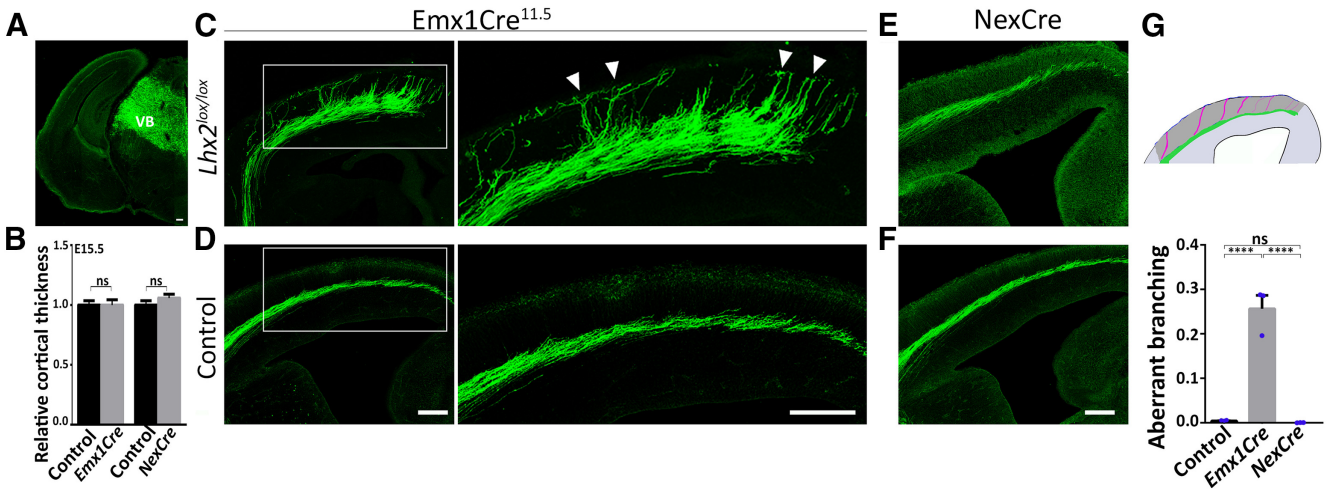

Figure 3. Embryonic thalamocortical axons are defasciculated and display premature growth into the cortical plate when *Lhx2* is disrupted using Emx1Cre, but not NexCre. ***A***, Electroporation of a plasmid encoding GFP into the diencephalon at E11.5 labels the thalamus and also thalamocortical axons by E15.5. ***B***, Cortical thickness is unaffected at E15.5 in *Emx1Cre*$^{11.5}$*::Lhx2*$^{lox/lox}$ and *NexCre::Lhx2*$^{lox/lox}$ brains. The average cortical thickness from the mutant sections was normalized to that of the respective controls. Ordinary one-way ANOVA; Control versus *Emx1Cre*$^{11.5}$*::Lhx2*$^{lox/lox}$, not significant, $p > 0.9999$; Control versus *NexCre::Lhx2*$^{lox/lox}$, not significant, $p = 0.8440$; *Emx1Cre*$^{11.5}$*::Lhx2*$^{lox/lox}$ versus *NexCre::Lhx2*$^{lox/lox}$, not significant, $p = 0.8440$. $n = 3$ brains for each genotype. ***C***, ***D***, Loss of *Lhx2* using Emx1Cre causes thalamocortical afferents to defasciculate as they course through the dorsal telencephalon at E15.5, whereas they remain tightly fasciculated in controls. In *Emx1Cre*$^{11.5}$*::Lhx2*$^{lox/lox}$ brains, thalamocortical axons enter the cortical plate prematurely and extend aberrantly up to the marginal zone (arrowheads). ***E***, ***F***, When *Lhx2* is disrupted using NexCre, thalamocortical afferents appear indistinguishable from those in the controls in E15.5 brains. ***G***, Sections of *Emx1Cre*$^{11.5}$*::Lhx2*$^{lox/lox,}$ *NexCre::Lhx2*$^{lox/lox}$ and control E15.5 brains were scored for aberrant axonal branching. Scatter dots in the bar plot represent aberrant branching value for each brain. Ordinary one-way ANOVA; Control versus *Emx1Cre*$^{11.5}$*::Lhx2*$^{lox/lox}$, $^{****}p < 0.0001$; Control versus *NexCre::Lhx2*$^{lox/lox}$, not significant, $p = 0.9992$; *Emx1Cre*$^{11.5}$*::Lhx2*$^{lox/lox}$ versus *NexCre::Lhx2*$^{lox/lox}$, $^{****}p < 0.0001$. $n = 3$ brains for each genotype. All fluorescence images are composites of multiple confocal images. ***C***, ***D***, Boxes represent regions displayed at high magnification in the adjacent panels. Scale bars, 100 μm.

Emx1Cre$^{11.5}$*::Lhx2*$^{lox/lox}$ mutant brains compared with controls as early as E17.5 (Fig. 2*C–G*). Other markers that delineate the borders of the VB *Chst2*, *Lhx9*, and *Prox1* also reveal this shrinkage at P0, whereas *Calb2* expression reveals no expansion of higher order thalamic nuclei (Fig. 2*E*) (Yuge et al., 2011; Frangeul et al., 2016; Kinare et al., 2019). The presence of cleaved Caspase3 indicates apoptosis in the VB at E18.5 and P0 (Fig. 2*F*). The dLGN appears unaffected by P0, but displays shrinkage by P7, together with the entire dorsal thalamus in mutant brains (Fig. 2*I*,*J*).

The VB shrinkage being apparent from E17.5 suggests that this is not because of any disruptions in corticothalamic input, since it is well established that projections from layer 6 do not enter VB until after E18.5 (Auladell et al., 2000; Jacobs et al., 2007). When we examined corticothalamic projections labeled by the Ai9 reporter in *Emx1Cre*$^{11.5}$ control and *Lhx2*$^{lox/lox}$ brains, the corticothalamic axons were detected in the reticular nucleus in both conditions and had not entered the dorsal thalamus (Fig. 2*H*).

The finding that the VB appears to be affected as early as E17.5 in *Emx1Cre*$^{11.5}$*::Lhx2*$^{lox/lox}$ mutants motivated the hypothesis that thalamocortical axons may display deficits in their development during the waiting period. Since the TCA-GFP line does not display detectable fluorescence at embryonic stages, we used *in utero* electroporation to label embryonic VB projections by transfecting a GFP-expressing plasmid into the diencephalon of control and mutant embryos at E11.5, when VB neurons are born. Control, *Emx1Cre*$^{11.5}$*::Lhx2*$^{lox/lox}$, and *NexCre::Lhx2*$^{lox/lox}$ brains were examined at E15.5, by which stage the dorsal thalamus expressed robust GFP expression (Fig. 3*A*). Cortical thickness at E15.5 was similar in control, *Emx1Cre*$^{11.5}$*::Lhx2*$^{lox/lox}$, and *NexCre::Lhx2*$^{lox/lox}$ brains (Fig. 3*B*). At E15.5, the thalamocortical tract coursed below the cortical plate in a tight bundle in control embryos, but in *Emx1Cre*$^{11.5}$*::Lhx2*$^{lox/lox}$ brains it displayed an exuberant ingrowth of thalamocortical fibers into the cortical plate at E15.5 (Fig. 3*C*,*D*). Furthermore, thalamocortical axons appeared defasciculated, extended several branches prematurely into the cortical plate, and extended aberrantly up to the marginal zone in *Emx1Cre*$^{11.5}$*::Lhx2*$^{lox/lox}$ brains (Fig. 3*C*, arrowheads). Such exuberant branching was not seen in E15.5 *NexCre::Lhx2*$^{lox/lox}$ brains, which displayed a well-ordered, bundled thalamocortical tract that coursed below the cortical plate, similar to controls (Fig. 3*E*,*F*). The area of the cortical plate in which green fibers were present was scored in each condition and found to be significantly increased in E15.5 *Emx1Cre*$^{11.5}$*::Lhx2*$^{lox/lox}$ brains compared with *NexCre::Lhx2*$^{lox/lox}$ and control brains (Fig. 3*G*).

The thalamocortical exuberant ingrowth phenotype was only seen when *Lhx2* is disrupted using Emx1Cre. Therefore, we reasoned that the critical requirement for this transcription factor must be in progenitors, not postmitotic neurons. Since essentially all cortical layers are produced sequentially from progenitors that express Emx1Cre, we sought to narrow down the stage at which LHX2 function is relevant for the proper guidance of thalamocortical axons, using tamoxifen-inducible CreERT2. Embryos of the genotype *CreERT2::Lhx2*$^{lox/lox}$ were electroporated with a GFP-expressing plasmid at E11.5 in the diencephalon to label the VB thalamocortical fibers, tamoxifen was administered at different stages to disrupt *Lhx2* (Fig. 4*C–F*), and the embryos were harvested at E15.5. Whereas tamoxifen administration at E11.5 closely recapitulated the defasciculation and exuberant ingrowth of thalamocortical axons seen in *Emx1Cre*$^{11.5}$*::Lhx2*$^{lox/lox}$ embryos (Fig. 4*B*,*C*,*G*), tamoxifen administration at E12.75 and at E13.5 resulted in a phenotype similar to control brains (Fig. 4*A*,*E*,*F*). Tamoxifen administration at E12.5 produced a phenotype mostly resembling that of control brains, except for a few fibers at dorsomedial levels that prematurely entered the cortex (Fig. 4*D*). Birthdating studies have established that subplate neuron production peaks at E11.5, but medially, the subplate also contains neurons born at E12.5 (Price et al.,

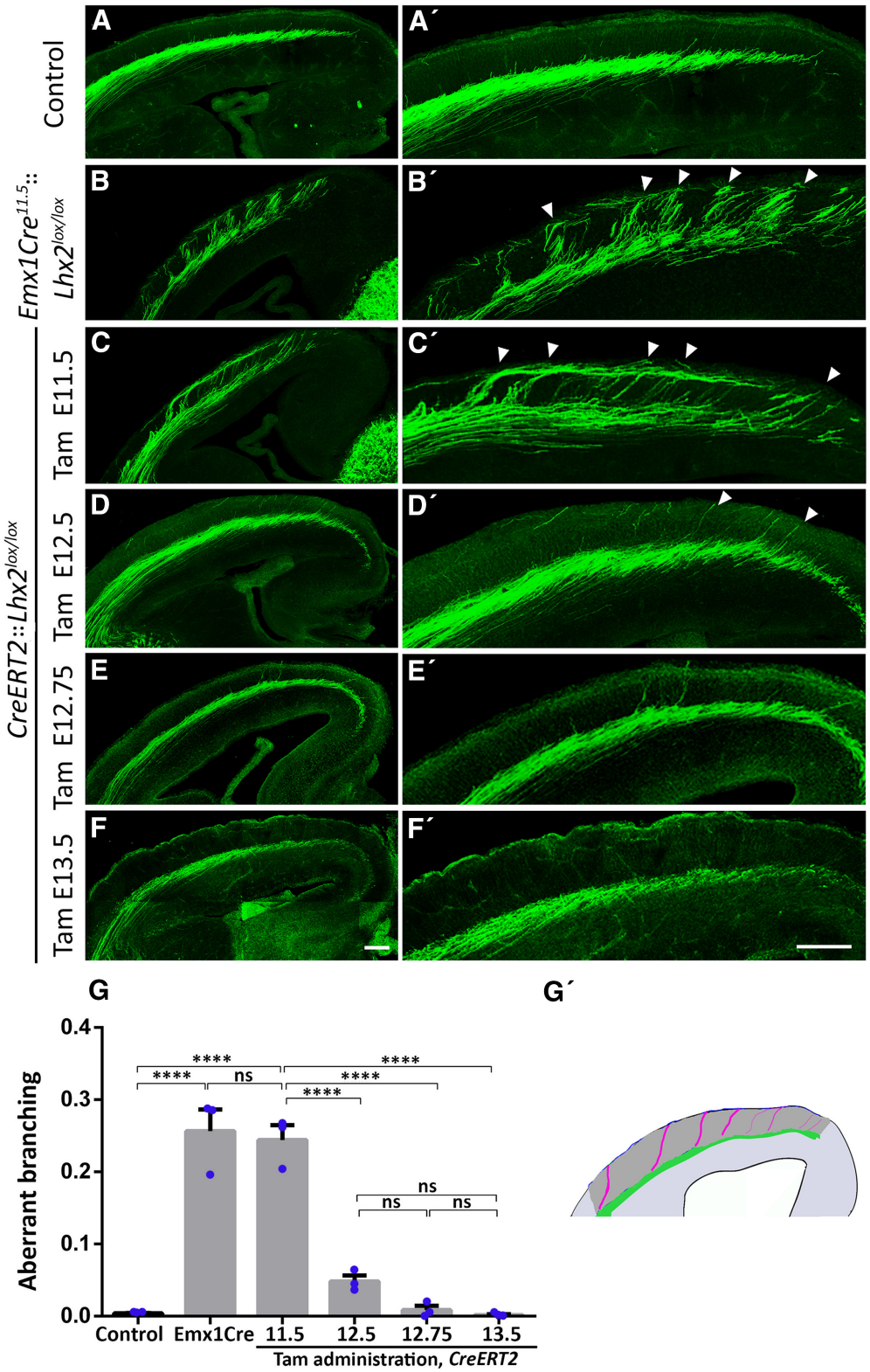

Figure 4. Early, but not late, cortical progenitors require LHX2 for normal thalamocortical innervation. ***A-F***, ***A′-F′***, Sections of E15.5 Control (***A***,***A′***), *Emx1Cre*$^{11.5}$*::Lhx2*$^{lox/lox}$ (***B***,***B′***), *CreERT2::Lhx2*$^{lox/lox}$ (***C-F***,***C′-F′***) brains in which thalamocortical innervation is visualized by electroporation of a plasmid encoding GFP into the thalamus at E11.5. ***A***, ***A′***, Thalamocortical afferents in control brains course in a tight bundle below the cortical plate (CP). ***B***, ***B′***, Loss of *Lhx2* using Emx1Cre causes premature ingrowth of thalamocortical afferents into the cortical plate that extend up to the marginal zone (arrowheads). ***C-F***, ***C′-F′***, This phenotype is recapitulated when tamoxifen is administered at E11.5 to *CreERT2::Lhx2*$^{lox/lox}$ but not E12.5, E12.75, or E13.5 (***D-F***). ***G***, ***G′***, Aberrant axonal branching of TCAs seen in *CreERT2::Lhx2*$^{lox/lox}$ Tam 11.5 brains is similar to *Emx1Cre*$^{11.5}$*::Lhx2*$^{lox/lox}$ brains. The exuberant branching phenotype is significantly reduced when tamoxifen is administered at E12.5, E12.75, or E13.5. Scatter dots in the bar plot represent aberrant branching value for each brain. Ordinary one-way ANOVA; Control versus *Emx1Cre*$^{11.5}$*::Lhx2*$^{lox/lox}$, ****$p < 0.0001$; Control versus *CreERT2::Lhx2*$^{lox/lox}$ Tam E11.5, ****$p < 0.0001$; *Emx1Cre*$^{11.5}$*::Lhx2*$^{lox/lox}$ versus *CreERT2::Lhx2*$^{lox/lox}$ Tam E11.5, not significant, $p = 0.9969$; $n = 3$ brains for each genotype. All panels are composites of multiple confocal images. ***A′-F′*** are high-magnification images of ***A-F***, respectively. Scale bars, 100 μm.

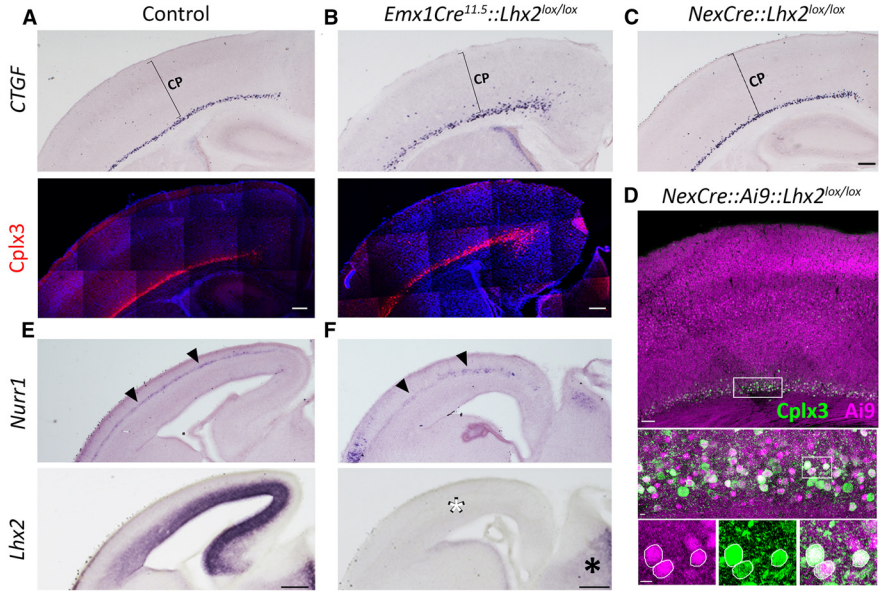

Figure 5. Subplate neurons are specified and positioned below the cortical plate upon Emx1Cre-mediated loss of *Lhx2*. ***A-C***, Expression of subplate markers in control, *Emx1Cre*$^{11.5}$*::Lhx2*$^{lox/lox}$, and *NexCre::Lhx2*$^{lox/lox}$ brains ($n = 3$ brains per condition). At P7, *CTGF* expression and CPLX3 immunoreactivity reveal a tightly packed subplate in controls (***A***) and *NexCre::Lhx2*$^{lox/lox}$ brains (***C***), but a less compact subplate in *Emx1Cre*$^{11.5}$*::Lhx2*$^{lox/lox}$ brains (***B***), located below the cortical plate (CP). ***D***, NexCre drives the expression of an Ai9 reporter in the cortical plate and also the subplate, which contains Ai9 and CPLX3-coexpressing cells in P7 *NexCre::Ai9::Lhx2*$^{lox/lox}$ brains. ***E***, ***F***, At E15.5, *Nurr1* is expressed in both control and *Emx1Cre*$^{11.5}$*::Lhx2*$^{lox/lox}$ subplate neurons (arrowheads). *Lhx2* expression is lost in the cortex of *Emx1Cre*$^{11.5}$*::Lhx2*$^{lox/lox}$ brains (white asterisk), whereas expression in the thalamus is maintained (black asterisk). The CPLX3 immunohistochemistry panels in ***A***, ***B*** and the low-magnification image in ***D*** are composites of multiple confocal images. Scale bars: ***A-C***, ***E***, ***F***, 200 μm; ***D***, low-magnification image, 100 μm; high-magnification images, 10 μm.

1997; Hoerder-Suabedisen and Molnár, 2013). Therefore, loss of *Lhx2* at the time of birth of subplate neurons correlates with the thalamocortical overshooting phenotype. LHX2 has multiple roles in this system: *Lhx2* mutant ventral telencephalic explants do not support normal topographic sorting of wild-type thalamocortical axons (Lakhina et al., 2007); loss of *Lhx2* using thalamus-specific driver Gbx2-CreERT2 (tamoxifen at E10.5) disrupts the topographic sorting of thalamocortical axons originating from specific thalamic nuclei, and results in occasional fibers overshooting the subplate (Marcos-Mondéjar et al., 2012). These results are distinct from our findings using the cortex-specific *Emx1Cre*$^{11.5}$, which indicate that LHX2 is necessary in early (E11.5) cortical progenitors at the time the subplate is being generated in order for normal thalamocortical axon projection to occur. In summary, our results suggest that daughter subplate neurons may develop aberrantly when LHX2 is absent in their mother cells, leading to abnormal subplate properties.

The phenotype of premature thalamocortical afferent ingrowth into the cortical plate with fibers reaching the marginal zone in the *Emx1Cre*$^{11.5}$*::Lhx2*$^{lox/lox}$ mutant was reminiscent of the thalamocortical projection phenotype described in *reeler* mutants, in which the subplate is mislocalized above the cortical plate (Molnár et al., 1998). Therefore, we examined whether the cortical subplate was specified and present in its correct location in mutant brains. We first examined the expression of *CTGF* (Connective Tissue Growth Factor) and CPLX3 (Complexin 3), established markers of the postnatal subplate (Hoerder-Suabedissen and Molnár et al., 2013). At P7, control brains displayed a tightly packed subplate expressing both markers (Fig. 5*A*). In *Emx1Cre*$^{11.5}$*::Lhx2*$^{lox/lox}$ brains, the subplate also expressed both markers (Fig. 5*B*). Furthermore, subplate cells were positioned normally, below the cortical plate, although they were not as tightly packed as in the controls. *NexCre::Lhx2*$^{lox/lox}$ brains also displayed a tightly packed subplate (Fig. 5*C*). In *NexCre::Ai9* brains, the Ai9 reporter was coexpressed with CPLX3, indicating that NexCre is indeed active in subplate cells (Fig. 5*D*). Neither *CTGF* nor CPLX3 are expressed in the embryonic subplate, so we used *Nurr1* (Nr4a2; Nuclear Receptor Subfamily 4 Group A Member 2), which labels the subplate at E15.5 (Fig. 5*E*,*F*). *Nurr1* expression reveals a less compact subplate in E15.5 *Emx1Cre*$^{11.5}$*::Lhx2*$^{lox/lox}$ brains than in controls; nonetheless, it is correctly positioned below the cortical plate when the thalamocortical axons arrive. We examined serial sections for *Lhx2* expression using a probe designed specifically against the floxed exon and confirmed that *Lhx2* expression was indeed lost from the entire cortex as expected for Emx1Cre-driven recombination (Fig. 5*E*,*F*). In summary, the premature thalamocortical ingrowth phenotype, with axons extending up to the marginal zone, cannot be explained by a mispositioning of subplate neurons in *Emx1Cre*$^{11.5}$*::Lhx2*$^{lox/lox}$ brains.

Although the position of the subplate in *Emx1Cre*$^{11.5}$*::Lhx2*$^{lox/lox}$ brains is not altered, it may be molecularly disrupted in a manner that is critical for thalamocortical axon guidance. To get an overall picture of the transcriptomic changes within subplate neurons on loss of LHX2, we performed RNA-seq on micro-dissected subplate tissue. We hypothesized that loss of LHX2 from the progenitor stage versus the postmitotic stage may have distinct regulatory consequences on the transcriptome of subplate neurons, and these differences may underlie the differences in the thalamocortical axon phenotype in *Emx1Cre*$^{11.5}$*::Lhx2*$^{lox/lox}$ and *NexCre::Lhx2*$^{lox/lox}$ brains. Therefore, we compared the wild-type subplate transcriptome with that of the *Emx1Cre*$^{11.5}$*::Lhx2*$^{lox/lox}$ and *NexCre::Lhx2*$^{lox/lox}$ subplate. We selected P0 as the stage of analysis because the last wave of cortical neurons has migrated past the subplate by this stage and would not be present in the dissected sample. The lowermost part of the cortical plate was visually identified in slices and micro-dissected, thus enriching the subplate population. The micro-dissection was confirmed by processing some slides for ISH for subplate marker CTGF (Fig. 6*A*). As expected, the transcriptomes of the *Emx1Cre*$^{11.5}$*::Lhx2*$^{lox/lox}$ and *NexCre::Lhx2*$^{lox/lox}$ subplate were each dysregulated compared with that of their corresponding littermate controls. We examined the genes that displayed a fold change >1.5 in each condition and found that 357 genes were differentially expressed in the *Emx1Cre*$^{11.5}$*::Lhx2*$^{lox/lox}$ subplate and 196 in the *NexCre::Lhx2*$^{lox/lox}$ subplate (Fig. 6*B*). However, when we compared these two differentially expressed datasets, only 29 genes were in common between the two (Fig. 6*B*). This indicated that, although both Cre drivers resulted in a loss of LHX2 from the subplate, using a driver that acts in progenitors versus postmitotic cells has vastly different consequences on the transcriptome of the resulting subplate neurons.

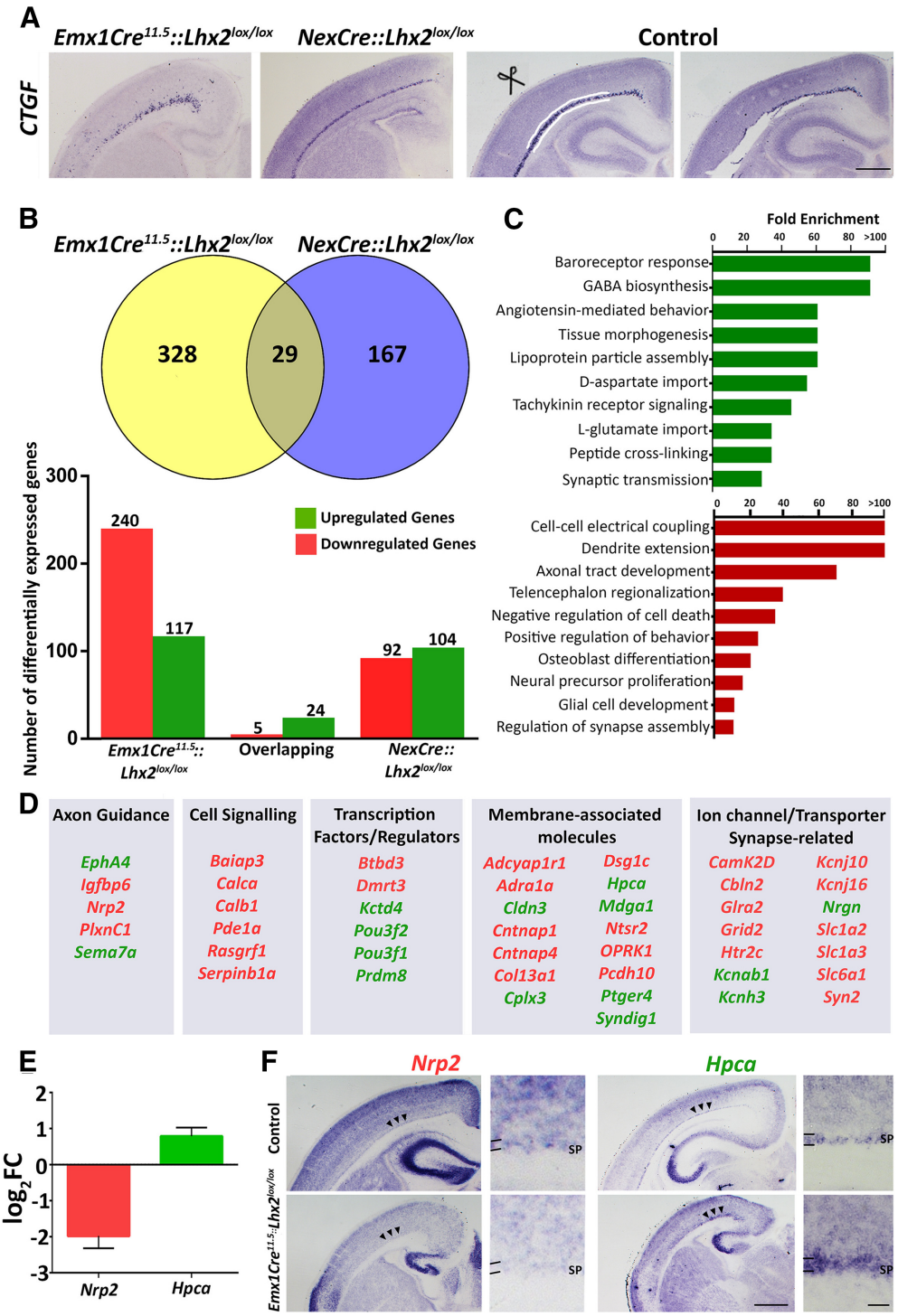

Figure 6. Transcriptomic analysis of the subplate. ***A***, *Emx1Cre*$^{11.5}$*::Lhx2*$^{lox/lox}$, *NexCre::Lhx2*$^{lox/lox}$, and control sections at P0 displaying *CTGF* expression in the subplate, and a control section in which the subplate was removed by microdissection. ***B***, Bulk RNA-seq revealed 328 and 167 differentially expressed genes unique to the *Emx1Cre*$^{11.5}$*::Lhx2*$^{lox/lox}$, *NexCre::Lhx2*$^{lox/lox}$ subplate, respectively, and 29 overlapping differentially expressed genes. ***C***, ***D***, GO analysis of the differentially expressed genes in the *Emx1Cre*$^{11.5}$*::Lhx2*$^{lox/lox}$ subplate (***C***) and selected genes in different functional categories (***D***; for related data, see Extended Data Figs. 6-1, 6-2, and 6-3). ***E***, Bar plot representing $\log_2$fold change values of representative differentially expressed genes *Nrp2* and *Hpca*. ***F***, *Nrp2* expression is decreased and *Hpca* expression is increased in the *Emx1Cre*$^{11.5}$*::Lhx2*$^{lox/lox}$ subplate (arrowheads). SP, Subplate. Scale bars: ***A***, ***F***, 500 μm; high magnification images in ***F***, 50 μm.

We further analyzed the 328 differentially expressed genes that were specific to the *Emx1Cre*$^{11.5}$*::Lhx2*$^{lox/lox}$ dataset. GO analysis revealed multiple developmentally significant gene clusters (Fig. 6*C*). We categorized these 328 dysregulated genes according to their known functions and found they encode molecules that mediate axon guidance, such as *EphA4*, *Nrp2*, *PlxnC1*, and *Sema7a*; cell signaling components; transcription factors; membrane-associated molecules, including protocadherin *Pcdh10*; as well as ion channels/transporters/synaptic molecules (Fig. 6*D*; Extended Data Fig. 6-3). These putative LHX2 targets suggest mechanisms by which the subplate could regulate the waiting of thalamocortical afferents. Several genes previously reported to be enriched in the subplate, such as

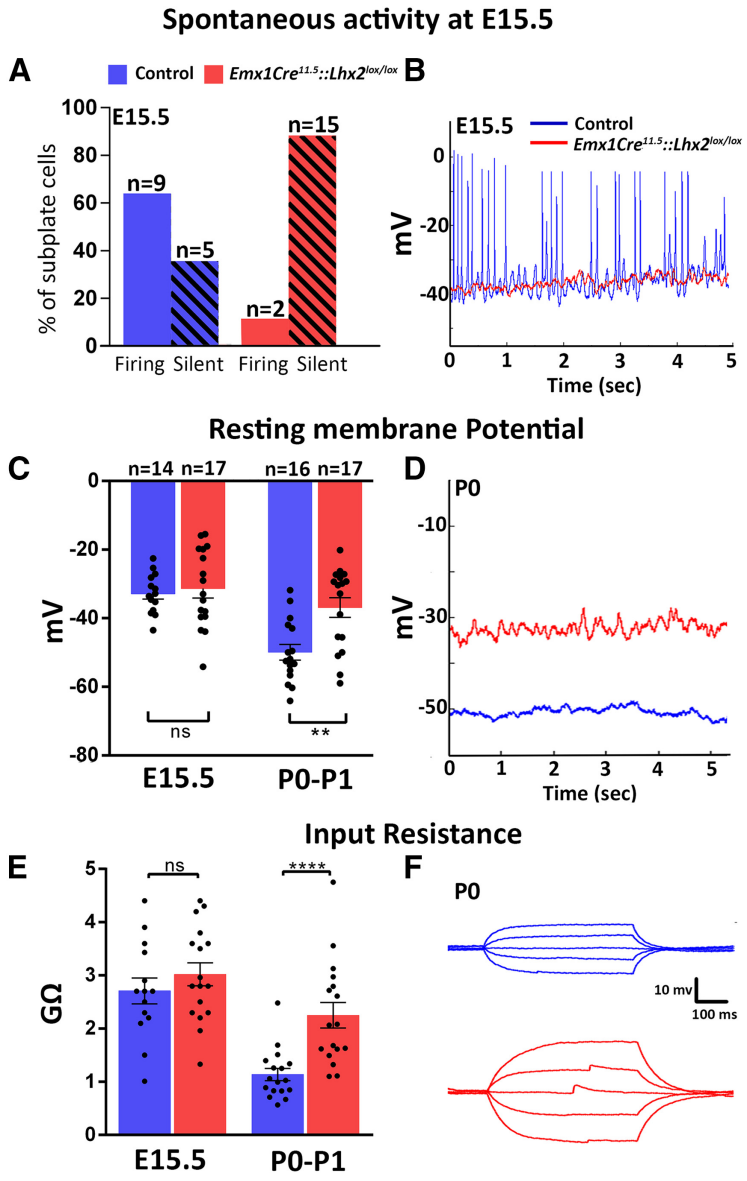

Figure 7. LHX2-deficient subplate neurons are electrically silent at E15.5 and electrophysiologically immature up to birth. ***A–F***, Spontaneous responses from slices of E15.5 control and *Emx1Cre*$^{11.5}$::*Lhx2*$^{lox/lox}$ brains. ***A***, The majority of control neurons fire regularly in absence of any current input, whereas the majority of mutant neurons are electrically silent. ***B***, Typical examples of mutant and control traces. ***C–F***, RMP and IR of subplate neurons from E15.5 and P0 control and *Emx1Cre*$^{11.5}$::*Lhx2*$^{lox/lox}$ slices. Both parameters are similar in mutant and control neurons at E15.5 but control neurons display a hyperpolarized RMP and lower IR by birth, which the mutant neurons do not (***C***,***E***). For E15.5, $n = 14$ cells were examined from 7 Control brains and $n = 17$ cells from 10 *Emx1Cre*$^{11.5}$::*Lhx2*$^{lox/lox}$ brains. For P0-P1, $n = 16$ cells were examined from 5 Control brains and $n = 17$ cells from 5 *Emx1Cre*$^{11.5}$::*Lhx2*$^{lox/lox}$ brains. Data are mean ± SEM. Individual values and statistical analyses are detailed in Extended Data Figure 7-1. $^{**}p \leq 0.01$. $^{****}p \leq 0.0001$. ***D***, ***F***, Typical examples of mutant and control traces at P0.

Hpca, *Syn2*, *Prdm8*, *Cplx3*, *Kcnab1*, *Pde1a*, *Sema7a*, *Kctd4*, *Adcyap1*, and *Pou3f1* (Hoerder-Suabedissen et al., 2009; Osheroff and Hatten, 2009; Oeschger et al., 2012), are dysregulated in the *Emx1Cre*$^{11.5}$::*Lhx2*$^{lox/lox}$ subplate. We used ISH to validate the RNA-seq results for some of these genes (Fig. 6*E*,*F*).

The RNA-seq analysis indicated that several genes involved in the bioelectrical properties of neurons were dysregulated in the *Emx1Cre*$^{11.5}$::*Lhx2*$^{lox/lox}$ subplate, for example, potassium channel subunits *Kcnab1*, *Kcnh3*, *Kcnj10*, and *Kcnj16;* a ligand-gated chloride channel subunit *Glra2*, an ionotropic glutamate receptor *Grid2*; and solute transporters *Slc1a2*, *Slc1a3*, and *Slc6a1*. This suggested to us that the electrophysiological properties of the subplate may be perturbed, and this may be relevant in the regulation of thalamocortical axon innervation of the cortex. A recent study demonstrates that subplate neurons are not only electrically active as early as E16, but they also form transient glutamatergic synapses on migrating multipolar neurons that will populate the cortical plate, which is critical to their multipolar-to-bipolar transition and subsequent migration (Ohtaka-Maruyama et al., 2018). These observations motivated an examination of whether the electrophysiological properties of subplate neurons were impaired on Emx1Cre-driven disruption of *Lhx2*. We prepared live slices from control and *Emx1Cre*$^{11.5}$::*Lhx2*$^{lox/lox}$ littermate embryos at stages at the beginning and the end of the waiting period, E15.5 and P0/P1. Subplate neurons were identified by their location between the cell-dense cortical plate with radially oriented neurons and the cell-sparse white matter, and their typical horizontal bipolar morphologies (Hirsch and Luhmann, 2008). First, we examined the intrinsic electrical properties of control and mutant subplate cells. Most control E15.5 subplate cells displayed a characteristic spontaneous firing pattern with only 36% being silent. In contrast, a larger fraction of mutant subplate neurons were silent (88%; Fig. 7*A*). The resting membrane potentials (RMPs) of mutant and control subplate neurons were similar at E15.5. While control neurons became hyperpolarized over time, mutant neurons failed to do so; by birth, their RMP was more depolarized compared with controls (Fig. 7*C*). We estimated input resistance by measuring membrane potential changes in response to a series of current steps (−10 pA to 10 pA, steps of 5 pA) and computing the slope (Fig. 7*E*,*F*). While the input resistance (IR) was similar in control and mutant subplate neurons at E15.5, control IR decreased by birth whereas mutant subplate cells continued to display a higher IR (Fig. 7*E*,*F*). Since a depolarized RMP and high IR are features associated with immature neurons (Cepeda et al., 2007; Valiullina et al., 2016), the *Lhx2* mutant subplate appeared to be electrically immature at birth.

Excitability, as assessed by measuring responses evoked by stepwise current injections, was reduced in *Emx1Cre*$^{11.5}$::*Lhx2*$^{lox/lox}$ subplate neurons compared with controls. At E15.5, the mutant subplate neurons were mostly limited to single spikes for input currents from 5 to 60 pA, whereas wild-type cells displayed a regular spiking pattern (Fig. 8*A*). At P0, although mutant subplate neurons displayed an improved spike frequency, it was lower than that of control neurons at input currents >35 pA (Fig. 8*B*). At both ages, the mutants displayed a higher proportion of single spiking neurons compared with regular spiking neurons (81% vs 21% at E15.5 and 33% vs none at P0; Fig. 8*C*). Mutant subplate neurons also displayed consistently lower spike amplitudes than controls (Fig. 8*D*). The current required to elicit spiking (rheobase) was higher for E15.5 mutant cells (Fig. 8*E*). After recording, biocytin-fillings revealed typical horizontal bipolar morphologies of subplate neurons in mutants as well as controls, at each age (Fig. 8*F*). In summary, the

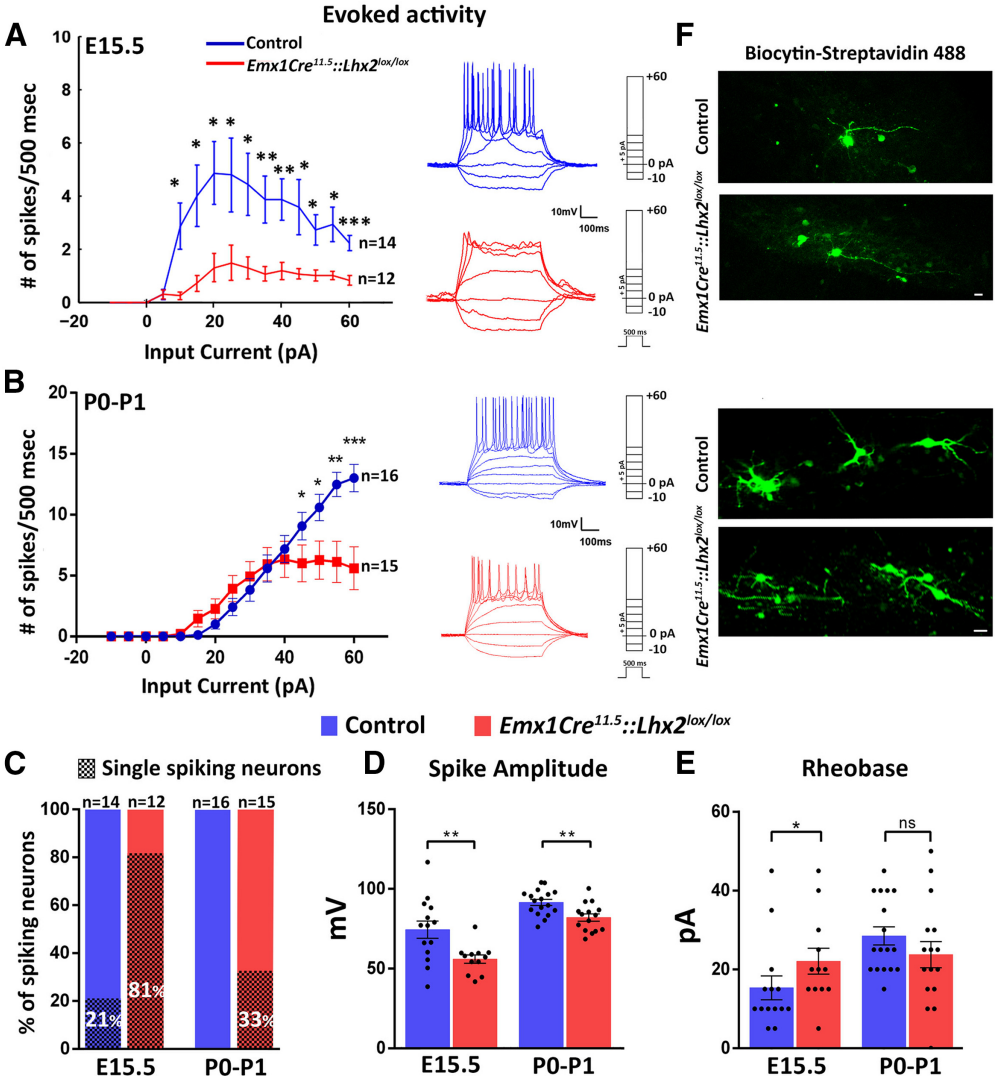

Figure 8. LHX2-deficient subplate neurons display attenuated evoked responses at E15.5 and birth. ***A–E***, Evoked responses from slices of E15.5 Control and *Emx1Cre*$^{11.5}$*::Lhx2*$^{lox/lox}$ brains. ***A***, ***B***, Mutant neurons have an attenuated spike frequency compared with controls at E15.5 and P0. Typical examples of mutant and control traces are shown adjacent to the line graphs. ***C***, The proportion of single-spiking neurons is greater in mutants compared with controls at E15.5 and birth. ***D***, Mutant neurons display decreased spike amplitudes at both stages. ***E***, Current injection required to elicit the first action potential is higher for E15.5 mutant neurons. Data are mean ± SEM. Individual values and statistical analyses are detailed in Extended Data Figure 7-1. *$p \leq 0.05$. **$p \leq 0.01$. ***$p \leq 0.001$. ***F***, Biocytin fills of mutant and control subplate neurons at the end of the recording reveal horizontal bipolar morphologies at both ages. Top, E15.5. Bottom, P0. Scale bars, 10 μm.

majority of subplate neurons in *Emx1Cre*$^{11.5}$*::Lhx2*$^{lox/lox}$ brains were electrically silent from E15.5, when the thalamocortical afferents first arrive. Their intrinsic bioelectrical properties failed to mature from E15 to P0, and their evoked responses were deficient, remaining typical of immature neurons at birth.

In summary, our results revealed dysregulation of diverse set of mechanisms in *Emx1Cre*$^{11.5}$*::Lhx2*$^{lox/lox}$ subplate neurons that could underlie the phenotype of premature exuberant overgrowth by the thalamocortical axons into the cortical plate and an eventual attrition of thalamocortical innervation of the postnatal cortex.

Discussion

The mechanisms that produce normally functioning subplate neurons are poorly understood. Our study offers insights into this process by highlighting an essential transcriptional regulatory function of LHX2 that operates in cortical progenitors at E11.5, when the subplate is born.

In order to identify the precise stage of progenitor that requires LHX2 function, and also to discriminate between progenitors versus postmitotic neurons, we used different Cre lines and compared the resulting phenotype with that seen in *Emx1Cre*$^{11.5}$*::Lhx2*$^{lox/lox}$ brains. NexCre-mediated *Lhx2* recombination does not recapitulate the Emx1Cre-mediated phenotype, since the thalamocortical axons wait at the subplate without showing aberrant innervation at E15.5. Therefore, we have uncovered a novel LHX2 function that selectively operates in progenitors and not in postmitotic neurons. Furthermore, when *Lhx2* recombination is induced via CreER, only tamoxifen administration at E11.5, but not E12.5- E13.5, recapitulates the Emx1Cre-mediated phenotype. Therefore, the previously reported phenotype of a reduced Tbr1-expressing layer 6, and an expanded Ctip2-expressing layer 5 in *Emx1Cre*$^{11.5}$*::Lhx2*$^{lox/lox}$ brains (Muralidharan et al., 2017) may not be relevant to the premature ingrowth of thalamocortical axons, since these cells are born primarily at E12.5 and E13.5, respectively. We

cannot, however, exclude a role of an E11.5 born cohort of layer 6 neurons that may participate in this phenotype.

Loss of LHX2 from E11.5 progenitors has profound consequences on the transcriptome and the bioelectrical properties of the subplate neurons which are born at E11.5. Since the subplate is the primary target of the thalamocortical pathway when it enters the dorsal telencephalon, we propose that loss of LHX2 in E11.5 progenitors results in a subplate with deficient molecular and electrophysiological properties such that the thalamocortical axons appear to overshoot it and enter the cortical plate prematurely. Alternatively, the subplate and E11.5-born layer 6 neurons may gain aberrant permissive properties on loss of LHX2 function, resulting in exuberant thalamocortical afferent ingrowth. Examples of dysregulated genes in the subplate that could affect thalamocortical ingrowth are molecules involved in axon guidance, membrane associated functions, such as cell adhesion, transcriptional control, and cell signaling, listed in Figure 6.

In this manner, molecular players acting downstream of LHX2 may control the temporary pausing of axonal growth and restarting subsequent reinnervation.

Interaction of thalamocortical and corticothalamic axons in the ventral telencephalon

The subplate plays a guidance role for the entry of the thalamocortical pathway into the dorsal telencephalon and for its initial trajectory below the cortical plate. In the *Tbr1* and *Gli3* mutants, the subplate appears to be absent altogether. The thalamocortical axons extend toward the pallial-subpallial boundary but fail to cross it, suggesting that interactions between subplate projections in the ventral telencephalon are required for thalamocortical afferents to enter the dorsal telencephalon (Molnár and Blakemore, 1995; Hevner et al., 2001; Bedogni et al., 2010; Magnani et al., 2013). Thalamocortical afferents target subplate neurons even when they are mislocalized. In the *reeler* mutant, cortical layering is inverted (Caviness and Sidman, 1973), and the subplate, identified by the expression of CTGF and CPLX3, is located above the cortical plate (a "superplate"). Thalamic axons extend through the cortical plate and reach the superplate and then turn downward to innervate layer 4 (Molnár et al,1998; Tissir and Goffinet, 2003). In the *p35* mutant, subplate neurons are located in the middle of an inverted cortical plate, in which earlier-born deep layer neurons are positioned above the subplate and later-born superficial layer neurons are positioned below the subplate. The thalamic axons enter the cortex obliquely toward the mispositioned subplate and eventually grow toward the marginal zone (Kwon and Tsai, 1998; Rakić et al., 2006). Together, these studies demonstrate that thalamocortical axons cannot cross the pallial-subpallial boundary without the presence of the subplate and will first target the subplate, even when it is mislocalized, underscoring its importance as a primary target.

In contrast to the mutants described above, in which subplate neurons are either absent or mislocalized, the subplate is correctly positioned below the cortical plate in *Emx1Cre*$^{11.5}$*::Lhx2*$^{lox/lox}$ brains. Corticothalamic projections reach the thalamus similar to wild-type brains, and thalamocortical fibers also navigate normally through the ventral telencephalon and cross the pallial-subpallial boundary. This suggests that the role of the subplate in guiding thalamocortical fibers into the dorsal telencephalon is unaffected. This mutant, therefore, serves as an excellent model to analyze mechanisms that control key subplate properties beyond its guidance function in terms of entry of thalamocortical axons into the dorsal telencephalon.

VB patterning and cortical area patterning

The defects we report in thalamocortical projections are not likely to be specific to the somatosensory modality, since the entire sensory cortex displays impoverished innervation from the thalamus in maturity (Shetty et al., 2013). In this study, we focused on the somatosensory thalamic nucleus and its projections to the cortex, but the role of the subplate is likely to be relevant to other thalamocortical projections as well.

Previous studies have shown that the VB is responsive to its connectivity with its target cortical area. When the primary somatosensory area (S1) is shifted to an extreme caudal location upon cortex-specific loss of *COUP-TF1*, the thalamocortical innervation targets the ectopic S1 and barrels are formed there (Armentano et al., 2007). When the S1 area is reduced as a consequence of cortex-specific loss of *Pax6*, or repatterned to a motor identity on cortex-specific loss of *Ctip1*, the VB undergoes selective repatterning and/or apoptosis (Zembrzycki et al., 2013; Greig et al., 2016). Similar mechanisms could explain why the VB continues to shrink postnatally in the *Emx1Cre:: Lhx2*$^{lox/lox}$ mutant (Fig. 2). Our study extends this target-dependent survival model further, in that VB shrinkage appears to begin embryonically, as a result of the thalamocortical axons encountering a subplate born from LHX2-deficient progenitors.

Progenitor-specific mechanisms regulate the properties of the postmitotic subplate

The subplate is described as the most mature neuronal population in the cortex since it is born first and achieves properties associated with mature neurons well ahead of the other cortical neurons (for review, see Luhmann et al., 2009). Synaptic transmission from subplate neurons plays an instructive role in multipolar to bipolar transition of migrating neurons in the developing cortex as early as E16 (Ohtaka-Maruyama et al., 2018). Thalamocortical axons are also known to make synaptic contacts with the subplate, which serves as a critical and necessary primary target of the thalamocortical pathway (Rakić, 1983; Ghosh et al., 1990; Ghosh and Shatz, 1992; Herrmann et al., 1994; Kanold et al., 2003; Kanold and Shatz, 2006; Tolner et al., 2012). Subplate neurons play distinct roles at different developmental stages; however, very little is known about the molecular mechanisms that regulate the properties of this population. These neurons are morphologically heterogeneous, ranging from inverted pyramidal neuron-like, to horizontal monotufted, bitufted, or multipolar with extensive arborization (Hanganu et al., 2002). Gene expression profiling of the subplate at different ages indicates tight temporal regulation of genes expressed specifically in the subplate (Hoerder-Suabedissen et al., 2009; Osheroff and Hatten, 2009; Oeschger et al., 2012).

The temporally dynamic and heterogeneous nature of the subplate is poorly understood. Our study uncovers an additional feature, that severe electrophysiological deficits manifest in postmitotic subplate neurons that are born from LHX2-deficient cortical progenitors from E15.5, when thalamocortical axons contact them. Furthermore, the transcriptome of the subplate arising from *Lhx2*-null progenitors shows gene dysregulation that has little overlap with that seen when LHX2 is lost postmitotically in those very cells. It is also striking that loss of LHX2 results in thalamocortical axons displaying inappropriate exuberant overgrowth only in the former but not the latter case. Recent work has shown that transcriptional priming of daughter neurons by their mother cells plays a critical role in setting the developmental trajectories during differentiation (Zahr et al., 2018; Telley et al., 2019). Our study motivates a broader investigation

of transcriptional and epigenetic controls in progenitors that control the properties of the resulting postmitotic progeny, eventually regulating how neurons participate in cortical circuitry.

References

Armentano M, Chou SJ, Tomassy GS, Leingärtner A, O'Leary DD, Studer M (2007) COUP-TFI regulates the balance of cortical patterning between frontal/motor and sensory areas. Nat Neurosci 10:1277–1286.

Auladell C, Pérez-Sust P, Supèr H, Soriano E (2000) The early development of thalamocortical and corticothalamic projections in the mouse. Anat Embryol (Berl) 201:169–179.

Bedogni F, Hodge RD, Elsen GE, Nelson BR, Daza RA, Beyer RP, Bammler TK, Rubenstein JL, Hevner RF (2010) Tbr1 regulates regional and laminar identity of postmitotic neurons in developing neocortex. Proc Natl Acad Sci USA 107:13129–13134.

Catalano SM, Shatz CJ (1998) Activity-dependent cortical target selection by thalamic axons. Science 281:559–563.

Caviness VS, Sidman RL (1973) Time of origin of corresponding cell classes in the cerebral cortex of normal and reeler mutant mice: an autoradiographic analysis. J Comp Neurol 148:141–151.

Cepeda C, André VM, Wu N, Yamazaki I, Uzgil B, Vinters HV, Levine MS, Mathern GW (2007) Immature neurons and GABA networks may contribute to epileptogenesis in pediatric cortical dysplasia. Epilepsia 48:79–85.

Chou SJ, Perez-Garcia CG, Kroll TT, O'Leary DD (2009) Lhx2 specifies regional fate in Emx1 lineage of telencephalic progenitors generating cerebral cortex. Nat Neurosci 12:1381–1389.

Frangeul L, Pouchelon G, Telley L, Lefort S, Luscher C, Jabaudon D (2016) A cross-modal genetic framework for the development and plasticity of sensory pathways. Nature 538:96–98.

Ghosh A, Shatz CJ (1992) Pathfinding and target selection by developing geniculocortical axons. J Neurosci 12:39–55.

Ghosh A, Antonini A, McConnell SK, Shatz CJ (1990) Requirement for subplate neurons in the formation of thalamocortical connections. Nature 347:179–181.

Goebbels S, Bormuth I, Bode U, Hermanson O, Schwab MH, Nave KA (2007) Genetic targeting of principal neurons in neocortex and hippocampus of NEX-Cre mice. Genesis 45:418–426.

Greig LC, Woodworth MB, Greppi C, Macklis JD (2016) Ctip1 controls acquisition of sensory area identity and establishment of sensory input fields in the developing neocortex. Neuron 90:261–277.

Hanganu IL, Kilb W, Luhmann HJ (2002) Functional synaptic projections onto subplate neurons in neonatal rat somatosensory cortex. J Neurosci 22:7165–7176.

Herrmann K, Antonini A, Shatz CJ (1994) Ultrastructural evidence for synaptic interactions between thalamocortical axons and subplate neurons. Eur J Neurosci 6:1729–1742.

Hevner RF, Shi L, Justice N, Hsueh Y, Sheng M, Smiga S, Bulfone A, Goffinet AM, Campagnoni AT, Rubenstein JL (2001) Tbr1 regulates differentiation of the preplate and layer 6. Neuron 29:353–366.

Hevner RF (2000) Development of connections in the human visual system during fetal mid- gestation: a DiI-tracing study. J Neuropathol Exp Neurol 59:385–392.

Hirsch S, Luhmann HJ (2008) Pathway-specificity in N-methyl-D-aspartate receptor-mediated synaptic inputs onto subplate neurons. Neuroscience 153:1092–1102.

Hoerder-Suabedissen A, Molnár Z (2013) Molecular diversity of early-born subplate neurons. Cereb Cortex 23:1473–1483.

Hoerder-Suabedissen A, Molnár Z (2015) Development, evolution and pathology of neocortical subplate neurons. Nat Rev Neurosci 16:133–146.

Hoerder-Suabedissen A, Wang WZ, Lee S, Davies KE, Goffinet AM, Rakić S, Parnavelas J, Reim K, Nicolić M, Paulsen O, Molnár Z (2009) Novel markers reveal subpopulations of subplate neurons in the murine cerebral cortex. Cereb Cortex 19:1738–1750.

Jacobs EC, Campagnoni C, Kampf K, Reyes SD, Kalra V, Handley V, Xie YY, Hong-Hu Y, Spreur V, Fisher RS, Campagnoni AT (2007) Visualization of corticofugal projections during early cortical development in a τ-GFP-transgenic mouse. Eur J Neurosci 25:17–30.

Jin XL, Guo H, Mao C, Atkins N, Wang H, Avasthi PP, Tu YT, Li Y (2000) Emx1-specific expression of foreign genes using "knock-in" approach. Biochem Biophys Res Commun 270:978–982.

Kanold PO, Shatz CJ (2006) Subplate neurons regulate maturation of cortical inhibition and outcome of ocular dominance plasticity. Neuron 51:627–638.

Kanold PO, Kara P, Reid RC, Shatz CJ (2003) Role of subplate neurons in functional maturation of visual cortical columns. Science 301:521–526.

Kinare V, Pal S, Tole S (2019) LDB1 is required for the early development of the dorsal telencephalon and the thalamus. eNeuro 6:ENEURO.0356-18.2019.

Kwon YT, Tsai L (1998) A novel disruption of cortical development in p35 (–/–) mice distinct from reeler. J Comp Neurol 395:510–522.

Lakhina V, Falnikar A, Bhatnagar L, Tole S (2007) Early thalamocortical tract guidance and topographic sorting of thalamic projections requires LIM-homeodomain gene Lhx2. Dev Biol 306:703–713.

Lebrand C, Cases O, Adelbrecht C, Doye A, Alvarez C, El Mestikawy S, Seif I, Gaspar P (1996) Transient uptake and storage of serotonin in developing thalamic neurons. Neuron 17:823–835.

Love MI, Huber W, Anders S (2014) Moderated estimation of fold change and dispersion for RNA-seq data with DESeq2. Genome Biol 15:550–521.

Luhmann HJ, Kilb W, Hanganu-Opatz IL (2009) Subplate cells: amplifiers of neuronal activity in the developing cerebral cortex. Front Neuroanat 3:19.

Lund RD, Mustari MJ (1977) Development of the geniculocortical pathway in rat. J Comp Neurol 173:289–305.

Magnani D, Hasenpusch-Theil K, Theil T (2013) Gli3 controls subplate formation and growth of cortical axons. Cereb Cortex 23:2542–2551.

Mangale VS, Hirokawa KE, Satyaki PR, Gokulchandran N, Chikbire S, Subramanian L, Shetty AS, Martynoga B, Paul J, Mai MV, Li Y, Flanagan LA, Tole S, Monuki ES (2008) Lhx2 selector activity specifies cortical identity and suppresses hippocampal organizer fate. Science 319:304–309.

Marcos-Mondéjar P, Peregrín S, Li JY, Carlsson L, Tole S, López-Bendito G (2012) The Lhx2 transcription factor controls thalamocortical axonal guidance by specific regulation of Robo1 and Robo2 receptors. J Neurosci 32:4372–4385.

Mizuno H, Luo W, Tarusawa E, Saito YM, Sato T, Yoshimura Y, Itohara S, Iwasato T (2014) NMDAR-regulated dynamics of layer 4 neuronal dendrites during thalamocortical reorganization in neonates. Neuron 82:365–379.

Molnár Z, Blakemore C (1995) How do thalamic axons find their way to the cortex? Trends Neurosci 18:389–397.

Molnár Z, Adams R, Goffinet A, Blakemore C (1998) The role of the first postmitotic cortical cells in the development of thalamocortical innervation in the reeler mouse. J Neurosci 18:5746–5765.

Molyneaux BJ, Arlotta P, Menezes JR, Macklis JD (2007) Neuronal subtype specification in the cerebral cortex. Nat Rev Neurosci 8:427–437.

Muralidharan B, Khatri Z, Maheshwari U, Gupta R, Roy B, Pradhan SJ, Karmodiya K, Padmanabhan H, Shetty AS, Balaji C, Kolthur-Seetharam U, Macklis J, Galande S, Tole S (2017) LHX2 interacts with the NuRD complex and regulates cortical neuron subtype determinants Fezf2 and Sox11. J Neurosci 37:194–203.

Oeschger FM, Wang W, Lee S, García-Moreno F, Goffinet AM, Arbonés L, Rakić S, Molnár Z (2012) Gene expression analysis of the embryonic subplate. Cereb Cortex 22:1343–1359.

Ohtaka-Maruyama C, Okamoto M, Endo K, Oshima M, Kaneko N, Yura K, Okado H, Miyata T, Maeda N (2018) Synaptic transmission from subplate neurons controls radial migration of neocortical neurons. Science 360:313–317.

Osheroff H, Hatten M (2009) Gene expression profiling of preplate neurons destined for the subplate: genes involved in transcription, axon extension, neurotransmitter regulation, steroid hormone signaling, and neuronal survival. Cereb Cortex 19:i126–i134.

Price DJ, Aslam S, Tasker L, Gillies K (1997) Fates of the earliest generated cells in the developing murine neocortex. J Comp Neurol 377:414–422.

Rakić P (1977) Prenatal development of the visual system in rhesus monkey. Philos Trans R Soc Lond B Biol Sci 278:245–260.

Rakić P (1983) Geniculo-cortical connections in primates: normal and experimentally altered development. Prog Brain Res 58:393–404.

Rakić S, Davis C, Molnár Z, Nikolić M, Parnavelas JG (2006) Role of p35/Cdk5 in preplate splitting in the developing cerebral cortex. Cereb Cortex 16 Suppl 1:i35–i45.

Schindelin J, Arganda-Carreras I, Frise E, Kaynig V, Longair M, Pietzsch T, Preibisch S, Rueden C, Saalfeld S, Schmid B, Tinevez JY, White DJ, Hartenstein V, Eliceiri K, Tomancak P, Cardona A (2012) Fiji: an open-source platform for biological-image analysis. Nat Methods 9:676–682.

Shatz CJ, Luskin MB (1986) The relationship between the geniculocortical afferents and their cortical target cells during development of the cat's primary visual cortex. J Neurosci 6:3655–3668.

Shetty AS, Godbole G, Maheshwari U, Padmanabhan H, Chaudhary R, Muralidharan B, Hou PS, Monuki ES, Kuo HC, Rema V, Tole S (2013) Lhx2 regulates a cortex-specific mechanism for barrel formation. Proc Natl Acad Sci USA 110:E4913–E4921.

Telley L, Govindan S, Prados J, Stevant I, Nef S, Dermitzakis E, Dayer A, Jabaudon D (2016) Sequential transcriptional waves direct the differentiation of newborn neurons in the mouse neocortex. Science 351:1443–1446.

Telley L, Agirman G, Prados J, Amberg N, Fièvre S, Oberst P, Bartolini G, Vitali I, Cadilhac C, Hippenmeyer S, Nguyen L, Dayer A, Jabaudon D (2019) Temporal patterning of apical progenitors and their daughter neurons in the developing neocortex. Science 364:eaav2522.

Tissir F, Goffinet AM (2003) Reelin and brain development. Nat Rev Neurosci 4:496–505.

Tolner EA, Sheikh A, Yukin AY, Kaila K, Kanold PO (2012) Subplate neurons promote spindle bursts and thalamocortical patterning in the neonatal rat somatosensory cortex. J Neurosci 32:692–702.

Valiullina F, Akhmetshina D, Nasretdinov A, Mukhtarov M, Valeeva G, Khazipov R (2016) Developmental changes in electrophysiological properties and a transition from electrical to chemical coupling between excitatory layer 4 neurons in the rat barrel cortex. Front Neural Circuits 10:1.

Wang CF, Hsing HW, Zhuang ZH, Wen MH, Chang WJ, Briz CG, Nieto M, Shyu BC, Chou SJ (2017) Lhx2 expression in postmitotic cortical neurons initiates assembly of the thalamocortical somatosensory circuit. Cell Rep 18:849–856.

Woolsey TA, van der Loos H (1970) The structural organization of layer IV in the somatosensory region (SI) of mouse cerebral cortex. Brain Res 17:205–242.

Yuge K, Kataoka A, Yoshida AC, Itoh D, Aggarwal M, Mori S, Blackshaw S, Shimogori T (2011) Region-specific gene expression in early postnatal mouse thalamus. J Comp Neurol 519:544–561.

Zahr SK, Yang G, Kazan H, Borrett MJ, Yuzwa SA, Voronova A, Kaplan DR, Miller FD (2018) A translational repression complex in developing mammalian neural stem cells that regulates neuronal specification. Neuron 97:520–537.e6.

Zembrzycki A, Chou SJ, Ashery-Padan R, Stoykova A, O'Leary DD (2013) Sensory cortex limits cortical maps and drives top-down plasticity in thalamocortical circuits. Nat Neurosci 16:1060–1067.

Zembrzycki A, Perez-Garcia CG, Wang CF, Chou SJ, O'Leary DD (2015) Postmitotic regulation of sensory area patterning in the mammalian neocortex by Lhx2. Proc Natl Acad Sci USA 112:6736–6741.